INSTITUTE OF PHYSICS
Department of Nuclear Physics
Slovak Academy of Sciences

.

PhD Thesis

Mgr. Juraj Kotulič Bunta

Bratislava, November 2003

Institute of Physics, Department of Nuclear Physics
Slovak Academy of Sciences

Juraj Kotulič Bunta

Asymmetric nuclear matter in the relativistic mean-field approach with hyperons and vector cross interaction

Supervisor: Ing. Štefan Gmuca, CSc.

It is in matter that we find the answer to our life. When we awake to the consciousness of matter, it is possible to free oneself from all shackles and widen consciousness beyond our habits, our knowledge and our little self.

Roshi Kaisen
Zen Buddhist Master

.

Contents

1 Introduction

In 1911 an existence of the atomic nucleus was revealed by Rutherford by bombarding of a gold-foil with α-particles. The weight of nucleus was explored by Thomson, who discovered also existence of isotopes. In 1932 the neutron was found by Chadwick, together with proton appearing to be the basic constituent of nucleus. It was natural to suppose an existence of another essential interaction binding protons and neutrons in nuclei - the strong interaction. Since that time it has been one of the basic problems and tasks of nuclear physics to understand its nature and principle, and, consequently, to describe the structure and properties of atomic nuclei.

The first qualitative features of the nuclear interaction was deduced from binding energies of light nuclei (mainly of deuteron - the only two-nucleon system bound), it turned out to be of a short-range and strong nature. There were performed first proton-proton scattering experiments in 30's which revealed its charge independence. The first more fundamental idea of strong interaction originated from Japanese physicist Hideki Yukawa in 1935. He suggested an existence of particle of medium mass (in comparison with nucleons) – meson – which should be responsible for intermediation of the strong interaction. Gravitational and electromagnetic interactions were the only forces known at that time, both having a simple mathematical form. However, the strong interaction proved to be much more complicated.

In 1937 the muon was found in cosmic radiation, interpreted as the particle proposed by Yukawa. Although the incorrectness of this assumption revealed later, it had supported the interest in Yukawa's idea. Finally, in 1947 the real meson, pion, was discovered in cosmic background, and soon after that also in Berkeley. The existence of a strong-interacting meson was motivation for the theoretical study of strong interaction in 50's. The pion appeared as a particle analogical to the photon in quantum electrodynamics. Based on QED success, ex-

pectations were strong. After decade of nucleon-nucleon scattering and deuteron research the pion (one-pion exchange) turned out to be a long-range part of strong interaction, while the shorter-range double-pion exchange was unable to describe empirical facts.

Building-up a phenomenological description of nuclear potential was a way out which was enabled by successful development of NN scattering experiments, that (contrary to the research of many-body system properties) offered more detailed information, especially in high energy scattering. Through these experiments an importance of spin and spin-orbit interaction was recognized. This period coincides with the first attempts of many-body system description in one-pion approach. Schiff [1] came with an idea that nuclear saturation could result from strong nonlinear self-interactions of scalar field. Johnson and Teller [2] showed that nucleon moving in potential created by a classical condensed field explained many empirical features of nuclear structure. Also Duerr [3] showed that using of the field theory considering vector and scalar mesons explained many finite nuclei properties.

In 1961 detection of heavier mesons became an important landmark in discovering the nature of strong interaction - ρ meson was found in Brookhaven and ω meson in Berkeley. The first product of this progress were OBE models (One Boson Exchange), based on Yukawa's conception of meson-intermediated nuclear interaction, and on the results of observations showing that mesons interacted also with themselves, with tendency to behave as a single particle of finite mass and quantum numbers. The most important of these correlation-induced contributions to strong interaction appeared to be a correlated 2π-exchange, simulated by the exchange of a single isoscalar-scalar meson (σ), being responsible for mid-range part of the interaction.

This fact together with the discovery of other mesons have influenced also description of many-body systems. Nuclear matter, a hypothetical infinite uniform system of nucleons, has become a subject of study. Due to several approxima-

tions which can be introduced for a description of such a system, mathematical solution of the problem is relatively simple. Nuclear matter is characterized by several parameters, e.g., binding energy per nucleon and saturation density. These empirical values are obtained from high-energy heavy-ion collision experiments, as well as from the study of heavy nuclei (by an extrapolation of charge and mass distribution) where the matter in their center is approximately the nuclear matter.

A great interest was paid to nonrelativistic description of many-body system. The base of this approach is the Hartree-Fock theory where nucleons move independently in a self-consistent single-particle potential originated from their interaction with other nucleons. The result is a set of single-particle wave functions. These calculations were also applied (considering of phenomenological two-particle potential reproducing the nuclear matter properties) to finite nuclei of the periodic table of elements. In spite of the successes of the nonrelativistic approach there remained some discrepancies between empirical observations and calculated results.

In 1974 an important progress was achieved when Walecka used a renormalizable field theory of baryons and mesons, characterized by finite number of coupling constants and masses [4, 5]. These can be calibrated to the observable nuclear properties, and then it is possible to extrapolate to high density and high temperature regions without any additional parameters. Since baryons and mesons are used as relevant degrees of freedom, the theory has been known as quantum hadrodynamics (QHD). Relativistic nucleon motion must be considered with increasing density as well as causal constraints. The reason for the relativistic treatment is also the fact that in spite of the apparently low nuclear binding energies which are only several per cents of the nucleon rest mass, this is due to a delicate balance between attractive scalar and repulsive vector potentials, both of the value of several hundreds of MeV. From above mentioned follows that the only approach unifying the required constraints is a local relativistic many-body

quantum field theory.

The most important contributions to the boson exchange potential come from an exchange of $\sigma(0,+,0)$, ω (1,-,0), η (0,-,0), ρ (1,-,1), π (0,-,1), and δ (0,+,1) mesons (with spin, parity, and isospin, respectively). Other mesons appeared to be less important, mostly due to their heavy masses and weak coupling constants.

Walecka's original idea was to create a fundamental theory of strong interaction where the mesons are quanta of field analogically to the role of photon in QED. However, nowadays the candidate for fundamental theory is the quantum chromodynamics (QCD) where gluons are the carriers of the interaction between quarks. From other features of this theory (asymptotical freedom, quark confinement) follows that QCD is simple and manageable only at short distances (high energies), and complicated at long distances (low energies). The meson theory can be understood as an effective description of quark-gluon dynamics in low-energy region. If the general lagrangian obeying QCD symmetries (Lorentz covariance, parity conservation, time inversion and charge-coupled invariance...) is constructed then the effective theory is general parametrization of the underlying quantum chromodynamics. The main reason for using such a low-energy approach is experimental observation of mesons and baryons. One of the goals of effective hadron theory is to reach better understanding of its previous successes in low energy region as well as their relation and connection to QCD. Another argument for developing the effective theories is the renormalization problem. The original Walecka's QHD model was renormalizable. Unfortunately, these renormalizable models have encountered difficulties due to large effects from loop integrals that incorporate the dynamics of the quantum vacuum [6]. The effective theory was an alternative.

Deeper understanding of the strong interaction is motivated not only by necessity of the nuclear structure and reaction description but also by observed astrophysical and cosmological phenomena. The situation is illustrated in Fig. 1. Existing atomic nuclei cover only narrow window of the nuclear equation of state

(EOS). However, astrophysics region supposes an existence of extreme phenomena, requiring knowledge of delicate details of the nuclear interaction behavior. Already in 1934 Baade and Zwicky [7] proposed an idea of neutron stars - objects with small radius and much stronger gravitational coupling than in the case of ordinary stars. Such a kind of stars rises from supernova explosions - one of the final periods of their evolution. The first models were developed by Oppenheimer and Volkov, describing neutron star matter as an ideal gas consisting of free neutrons. Most of the works on neutron stars at that time were based on an idea that neutron cores of ordinary stars are the source of their energy. However, after understanding of thermonuclear synthesis, interest in this field fell down.

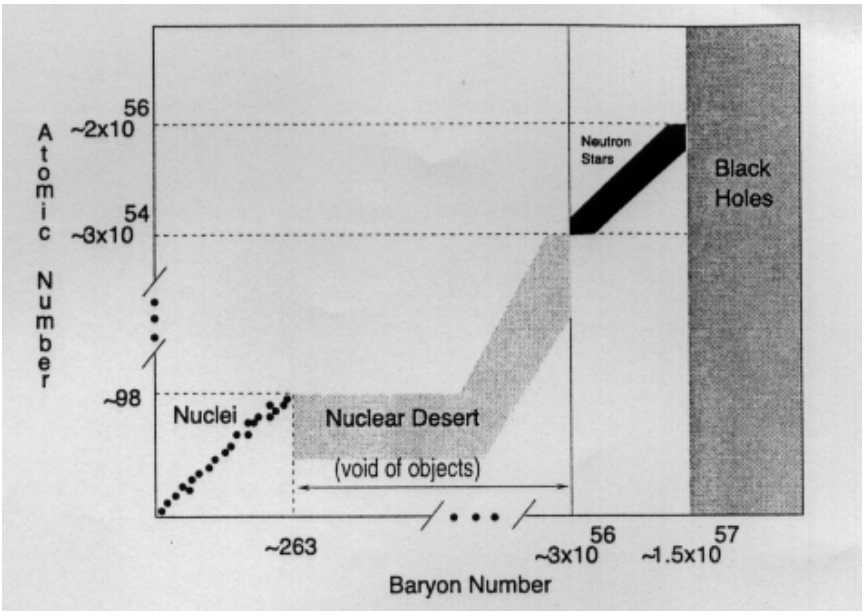

Figure 1: Connection between finite nuclei and stellar configurations, being in principle giant atomic nuclei, is apparent also from this illustration.

Discovery of cosmic sources of röntgen radiation [8] refreshed this area of nuclear interaction applications. The finding was interpreted as an observation of a young neutron star and many models of neutron stars and their evolution have emerged. However, many theoreticians did not believe in an existence of such extreme objects. Situation changed in 1967 when the pulsars [9] were discovered.

Nowadays, it is generally accepted that pulsars are rapidly rotating neutron stars. A pulsar in supernova explosion remnants was revealed, thus confirming theory of pulsars' birth process. Observing pulsars in binary systems enabled empirical determination of their mass.

Due to the recent developments both in the theoretical and experimental nuclear physics and astrophysics, it is inevitable to improve the models describing nuclear systems. This work deals with nuclear matter properties calculations in the mean-field theory. The nuclear matter is a starting point for description of other phenomena and processes. Since new accelerator facilities produce nuclei with high isospin asymmetry and nuclear matter at densities of several times of the saturation density, and developing astrophysical observations of compact objects consisting from highly asymmetric nuclear/baryon matter have been performed, it is useful to enhance the isovector description of nuclear matter. This work fulfils this aim through incorporation of isovector scalar δ meson as well as by cross interaction between vector ω and ρ mesons. The parametrizations obtained by fitting procedure to the more fundamental Dirac-Brueckner-Hartree-Fock theory (which is, however, not applicable to finite nuclei calculations yet) represent an effective description of asymmetric nuclear matter applicable also to finite nuclei calculations. The role of the cross interaction is examined, both in asymmetric nuclear matter and neutron star matter (nuclear matter containing also hyperons and leptons in β-equilibrium).

This work consists of introduction where a brief historical overview has been given. The second section describes an outline of recent status of the finite nuclei and nuclear matter description problems and also closely related (astrophysical) topics. The theoretical framework of the mean-field theory is then given, including vector cross interactions as well as hyperon and lepton incorporation in β equilibrated matter. The goal draft follows. The obtained results are analyzed in detail in the next two sections. Summary and outlook are presented in the end of work.

2 Recent Developments

Several physical phenomena provide information about nuclear structure and NN interaction. The scattering of medium-energy nucleons, employing the Dirac-Hartree description of the nucleus together with the relativistic impulse approximation (RIA) [10], is one of them. Interaction between projectile and target which is assumed to have the same form as the interaction between free nucleons, is used to produce a nucleon-nucleus optical potential.

The effective field theories (developed due to difficulties of renormalizable QHD theories, as mentioned in introduction), rely on the observation that it is not necessary to explicitly include dynamics at significantly shorter length scales than that are relevant for phenomena examined. The effects of degrees of freedom corresponding to shorter length scales are implicitly contained in coupling parameters in the effective theory, by fitting these parameters to experimental data. A well-known application of the effective theory is chiral perturbation theory in which one observes that the spontaneous breaking of chiral symmetry in QCD implies that Goldstone boson such as pions are the relevant degrees of freedom in the low-energy region [11]. Studies of two- and many-body systems are under investigation now [12].

Generally theoretical activities in the field of nuclear many body theories can be grouped into three different approaches: *ab initio* methods; self-consistent mean-field (MFT) and shell-model theories; and macroscopic models with microscopic shell corrections. Nuclear MFT are partially analogical to density-functional theory [13] which gives a successful description of many-electron systems.

The starting point of *ab initio* methods is a given nucleon-nucleon potential - an effective interaction for description of nucleon-nucleon scattering data. Its characteristic features are strong repulsive core, thus the nuclear matter behaves as a strongly correlated quantum liquid. Such a description requires highly sophis-

ticated many-body theories, for example, Dirac-Brueckner-Hartree-Fock [5, 14] that provide a direct connection of two-nucleon problem and nuclear matter properties. However, due to its complexity it is not applicable to finite nuclei calculations at present. Another possibility is an usage of correlated basis functions [15]. Nuclear saturation properties are well reproduced by all these treatments. There is, however, a distinction - the nuclear matter saturation is appropriately reproduced also quantitatively only by models which employ not only nucleon-nucleon interaction, but also additional empirical three-body force. Continuous investigation is being run nowadays, trying to use connections from underlying QCD [16] to explain the microscopic origin of this force, and recently also by intrinsic nucleonic degrees of freedom.

The average features of nuclear binding energies are described sufficiently by macroscopic nuclear liquid-drop model [17]. The energy is parameterized in terms of the global properties such as volume energy, asymmetry energy, surface energy etc. Additionally, using a phenomenological single-particle potential, a correction energy is calculated from single particle spectrum, and this microscopic-macroscopic method has reached high descriptive power. A large amount of *ad hoc* modelling, however, strongly limits the extrapolation capabilities of this model.

Another model working at microscopic level but employing also effective interactions is the shell-model. In this approach one takes for the mean-field a standard phenomenological single-particle model but then performs a configuration-mixing calculation involving all many-body states that can be constructed using a broad band of single-nucleon states around the Fermi energy [18]. The residual interaction in the active space is usually fitted phenomenologically, and also problem of proper saturation point is avoided by using a phenomenologically prescribed mean field. Due to rapidly growing dimension with system size the Monte Carlo techniques or specific diagonalization methods have been developed for heavier nuclei.

On the other hand, the mean-field theories concentrate on self-consistent determination of the nuclear mean field. The effective interactions are used in the mean-field calculations. Actual parameters are adjusted by fits to nuclear structure data. After passing through problem of symmetry of the wave function which had limited application of the model to ground-state properties of even nuclei, studies of properties of heavy nuclei could be systematically performed. Experimental developments increasing our knowledge of nuclei far from stability have also significantly contributed to improvement of effective interactions. Nowadays, one has to introduce correlations beyond the mean field to improve further the description quality of this very successful model.

Generally, the mean-field models deal with a potential well of nucleons computed from the nucleonic wave functions. This is theory at the level of Hartree-Fock approximation. This is inadequate for a description of nuclear properties that are strongly influenced by pairing correlations. Generalization of the mean-field concept including a pairing field, calculated with the Hartree-Fock-Bogoliubov (HFB) equations [19], takes these correlations into account.

Widely used method for time-reversal-invariant systems is the BCS approximation. However, due to required knowledge of pairing partner states it is well defined only in the case of time-reversal invariance. In such systems a much simpler calculation scheme is generated, and it is the reason that the BCS is introduced for such systems.

The basic idea of microscopic-macroscopic approaches is a separation of total energy into the smooth background energy and the shell-correction energy. It is calculated from single-particle energies obtained either from parameterized single-particle models (modified harmonic oscillator, Woods-Saxon or folded Yukawa potentials) or from fully self-consistent mean-field calculations where this shell-correction energy appears as an useful tool for analyzing MFT models and parametrizations [20]. The background energy then has to be parameterized with the highest possible accuracy. A direct connection of self-consistent MFT

and micro-macroscopic models is obtained by means of semiclassical approximations. The simplest one is the Thomas-Fermi model and extended Thomas-Fermi model [21]. This model is able to describe many local features of self-consistent MFT models. References to many relativistic and extended Thomas-Fermi works can be found in Ref. [22].

Due to a present incapability to perform full *ab initio* calculation of finite nuclei, one employs effective interactions. The short range of nuclear interaction and the long wavelength of the single-nucleon states suggest an expansion in terms of zero-range interactions which is called density-matrix expansion and provides formal derivation framework for the Skyrme energy functional [23]. It is necessary to obtain an effective two-body interaction, e.g. from Brueckner-Hartree-Fock microscopic force. The derivation of parameters of the expansion from the given Brueckner-Hartree-Fock calculations has provided a fair reproduction of nuclear properties in subsequent mean-field calculations [24] but it fails quantitatively. It could be the problem of local-density approximation itself or of the Brueckner-Hartree-Fock calculations but this question has not been answered clearly yet.

2.1 Effective Interactions

Three standard models are used for the nuclear mean field - based on Skyrme interactions [25], Gogny force [26] and relativistic mean-field model [4].

The Skyrme Hartree-Fock approach employs zero-range interaction. The total binding energy in the Skyrme Hartree-Fock approach is given by the sum of the kinetic energy, the Skyrme energy functional which models the effective interaction between nucleons, the Coulomb energy, the pair energy and corrections for spurious motion. Due to local nature of the Skyrme energy functional, it has several technical advantages. The number of integrations required for solutions of Skyrme Hartree-Fock equations is significantly reduced because of the same structure of exchange and direct terms. There are two basic concepts to derive the Skyrme energy functional. The first one is a derivation from the Hartree-

Fock expectation value of the zero-range momentum dependent two-body force introduced by Skyrme. Almost all the Skyrme forces are well known to have unrealistic pairing properties. This strict approach is thus rarely used, and the contributions to the pair energy are dropped. Additionally, it introduces many dependencies among the coupling constants that lead to some difficulties. For instance, the usual parametrization of a three-body force which was used in some early parametrizations to derive the density-dependent term, causes a spin instability in the infinite nuclear matter and finite nuclei, a problem which persists even in recent parametrizations. The second concept is parametrization of energy functional directly without reference to an effective two-body force. It is free of all previous mentioned difficulties. Free parameters are coupling constants of the energy functional not fixed by global symmetries. Also particle-hole and particle-particle (pairing) channels of the effective interactions are decoupled. The only disadvantage is that the additional coupling constants have to be adjusted to the data and only few applications have tried this so far.

The interpretation of the Skyrme interaction as an energy density functional endows the spin-orbit interaction with a more flexible isospin structure. The new forces were thus constructed [27] differing from the standard Skyrme Hartree-Fock forces in the extrapolation of shell structure to exotic nuclei. The difference in spin-orbit force between standard relativistic mean-field and the Skyrme energy functional in a nonrelativistic limit is not made by its isospin dependence only, but also by its density dependence. This degree of freedom was explored in Ref. [28].

In the first Skyrme interactions a power of density dependence $\alpha = 1$ was used, however, this yielded too large incompressibility. The simple generalization from 1 to α has been the most efficient way, although many other generalizations have been tried. Nonetheless, all generalizations of density dependence performed so far were formulated within the Hartree-Fock expectation-value approach to the Skyrme energy functional which leads to the interrelations between coupling

constants and also adds density dependencies in unwanted places.

While the standard relativistic mean-field model has finite range couplings through exchange of mesons, the Skyrme Hartree-Fock method uses strictly point couplings. However, there is a variant of the Skyrme Hartree-Fock which merges the gradient term with the zero-range two-body force into a finite-range two-body coupling. Recently also an alternative approach has been developed [29]. Whereas the Skyrme functional can be viewed as a systematic expansion in derivatives up to second order with usually simple density dependence, this alternative approach's functional omits the terms containing derivatives except for the spin-orbit interaction and employs much more elaborate density dependence for all remaining terms.

Unlike the Skyrme Hartree-Fock, the Gogny force employs a finite range interaction. However, there was not reached a correct reproduction of binding energies at the Hartree-Fock level of approximation. It was thus suggested to add a density dependence in the interaction and also spin-orbit term. The divergence of zero-range pairing model is avoided and that enables one to use Gogny interaction simultaneously in both mean-field and pairing channels. The interaction has been adjusted with the direct Coulomb and Coulomb exchange terms calculated exactly.

Widely used and powerful tool for describing various aspects of many body problem - the mean-field theory [5, 30] - provides an elegant and economic framework for calculation. The first attempts were nonrelativistic ones, however, due to empirically proved existence of large scalar and vector fields in nucleon-nucleon interaction comparable with nucleon mass, it appeared necessary to take into account relativistic effects. Relativistic treatments have several advantages, for example, natural incorporation of the spin-orbit force [5], shift of the saturation curve - the so-called "Coester band" - towards the empirical values [14], the successful description of finite nuclei [31], etc. The nonlinear MFT approach [32] has already been proven to be a reliable tool for the calculations of finite nuclei prop-

erties in the valley of stability. By reason that new experimental capabilities have been developed by a continual improvement of particle accelerators, it is available nowadays to measure properties of exotic nuclei with high isospin asymmetry. Additionally, increasingly more precise observations and measurements of properties of neutron stars and supernovae have been carried out. This naturally brings a need for a better description of isospin degree of freedom, which can be done by enhancing the isovector meson sector. The isovector scalar δ-meson was included into MFT in Ref. [33] for this purpose and recently also cross interactions between isovector and isoscalar fields have been introduced [34], being studied also in this work. The basic concept of MFT is building the many-body state as an independent quasiparticle state from single-particle wave functions which are four-component Dirac spinors. The interaction through meson fields is considered to be an effective one. One has a choice to use effective zero-range forces (point couplings) and much more frequently used effective finite-range interactions. Assuming nucleus to be a system of interacting nucleons and mesons, the effective interaction is introduced through Klein-Gordon equations for the meson fields which are coupled to the Dirac equations for the nucleons. Using several approximations, these equations are solved selfconsistently. Either through nonlinear self-couplings of meson fields or through density-dependent coupling constants (or through a combination of both) one can also model a density dependence. More detailed information about mean-field framework will be given in the third section of this work.

There are also several alternatives to this model, mostly motivated by its particular defections. For example, derivative tensor couplings of the vector fields are used within the standard relativistic mean-field approach [35], and derivative couplings of the scalar field were introduced in Ref. [36].

An alternative to nonlinear couplings in terms of the density-dependent coupling constants have been suggested [24], known as density-dependent mean-field model. Relativistic Hartree-Fock models of nuclear matter and finite nuclei are

described in Ref. [37, 38]. The role of pion is discussed in Ref. [39], relativistic density-functional theory for nuclei is analyzed in Ref. [40]. Also a point coupling model has been explored recently [41]. However, these models does not approach yet in quality the standard model.

Model of strong interaction needs to contain also the Coulomb interaction. All relativistic mean-field forces and also the early Skyrme Hartree-Fock forces incorporate the direct Coulomb term only.

Another important feature is represented by pairing correlations. A widely used effective pairing interaction is a zero-range local force, often including a density dependence. This simple form of interaction was introduced in 1970's [42]. All pairing models blur the occupation of single-particle levels close to the Fermi surface. Thus the dominant contribution comes from the nuclear surface. The strength of pairing force depends on isoscalar effective mass and is adjusted phenomenologically to reproduce the odd-even staggering of energies in selected nuclei. Also more complicated pairing interactions were used by adding several terms for density derivatives to a density-dependent interaction. Deriving a relativistic theory of pairing has been an important progress of recent years, also with its application to finite nuclei [43]. However, calculations using pairing interactions do not converge generally, hence a prescribed cutoff has to be complemented. There are slight differences among cutoff recipes used in different methods.

2.2 Correlations Beyond the Mean-Field

The bulk properties of many nuclei are well described by the static mean-field approach discussed above. However, to achieve higher precision or to describe larger set of data one has to consider additional correlations. It is possible through various concepts. The first is *the generator coordinate method* which is closely related to multi-configurational Hartree-Fock method used in atomic physics and also to Monte Carlo shell model in nuclear physics. Second one is the *path-integral method*, where both methods allow to deal with large-amplitude collective

motions that appear to be the most important correlation effect. The third method are *diagrammatic methods* which are also useful for collective motion study.

The generator coordinate method was one of the first attempts to incorporate both collective and single-particle nuclear dynamics [44]. It can describe a wide range of phenomena and it has improved out understanding of the connection between phenomenological models of collective motion and microscopic approaches (e.g., Hartree-Fock). Moreover, thanks to the approximations of this method such as the Gaussian overlap approximation which is an intermediate step of connection between generator coordinate method and Schrödinger equation, it is possible to make links between microscopic models and collective models. They have been used to determine simple rotational and variational corrections to mean-field results.

A characteristic feature of the many-body problem study is an existence of symmetries. They introduce relations between the single-particle wave functions. While self-consistent mean-field wave functions are often constructed in a superposition manner, they break symmetries of nuclear Hamiltonian and these symmetries associated with zero excitation energy and large-amplitude motion have to be restored. One possibility is using of *particle-number projection* with variation after projection [45] that arises from the BCS states not being eigenstates of the particle-number operator, and is useful in description of, e.g., fast rotating nuclei. It is often advantageous to use also the Lipkin-Nogami approximate scheme for particle-number projection [46]. Similarly, since the deformed mean-field states are not eigenstates of the total angular momentum, the *angular momentum projection* is used [47], together with several additional approximations [48] satisfactorily describing properties of deformed nuclei. The last, but very important restoration procedure is *center-of-mass projection* [49], induced by broken translational invariance following from localization of mean field in space. The relative contribution of center-of-mass correction to the total bind-

ing energy is the largest for light nuclei since its value decreases with increasing nucleon number and vanishes for infinite nuclear matter.

A straightforward extension of stationary mean-field models is represented by the time-dependent mean-field methods. There are various approaches: *time-dependent density-functional theory* [50], in the nuclear dynamics known as *the time-dependent Hartree-Fock* (TDHF), or *the time-dependent Hartree-Fock-Bogoliubov* (TDHFB) in the case of pairing. There are many applications of these methods, e.g., in nuclear and heavy-ion dynamics [51]. Limiting cases are often considered, for example, the low-energy region of surface vibrations and fission is reached by adiabatic TDHF. The TDHFB is a starting point for quasiparticle Random-Phase Approximation (QRPA), due to its first derivation with diagrammatic techniques [52] being a basic theory of nuclear excitations in the regime of giant resonances. There exists many different notations for the RPA equations and techniques for their solution. Since one is often interested only in few key data, many simplifications such as sum-rule approaches are also used. One has also to note that there are some problems in connection with energy functionals and usual practise is to ignore RPA correlations, since they are supposed to be contained in the energy functional, and to consider only RPA excitations.

2.3 Parametrizations

Several bulk properties of finite nuclei and key features of nuclear matter are used as a phenomenological input for adjusting of the effective forces. Probably the most paramount one is the total binging energy of nucleus which can be obtained by numerical solutions of the mean-field equations, corrected also for spurious motion. Nuclear structure can be well analyzed by using the nuclear charge density which provides information about nuclear shape and is determined by elastic electron scattering. Due to a need for considering also intrinsic electromagnetic structure of the nucleons, one has to take into account also the proton and neutron densities individually. Most of the information contained in the charge form

factor at low momentum can be described by root-mean-square radius, the (first) diffraction radius and surface thickness. By reason that calculation of charge rms radius from full charge form factor is difficult, approximations are often used for simplification [53]. Another related quantity directly accessible from experiments is the isotopic shift of charge mean-square radii. The most important quantity affecting the charge distribution is proton distribution, however, also neutron distribution provides useful information.

Effective interactions are widely characterized also by infinite nuclear matter properties. Important features are energy per particle (often called equation of state) with its minimum at saturation density, then incompressibility of matter corresponding to the curvature around saturation point and related to, e.g., giant monopole resonance. Isovector curvature at saturation point determines the symmetry energy, and due to quasiparticle nature of mean-field models, an important quantity is also nucleon effective mass. For more detailed information and theoretical definition of these quantities see the next section of this work. The actual values of infinite nuclear matter properties are listed in Tab. 1.

Table 1: Properties of nuclear matter for various parametrizations: binding energy E_b at saturation density ρ_B^{sat}, incompressibility K_∞, and nucleon effective mass fraction m^*/m. Adapted from Ref. [55].

Parametrization	ref.	$E_b[MeV]$	$\rho_B^{sat}[fm^{-3}]$	$K_\infty[MeV]$	m^*/m
SIII	[56]	-15.93	0.145	356	0.76
SkM*	[57]	-15.86	0.161	218	0.79
SkP	[58]	-16.03	0.163	202	1.00
SLy6	[59]	-15.92	0.159	230	0.69
SkI4	[27]	-15.92	0.160	248	0.65
BSk1	[60]	-15.80	0.157	231	1.05
D1S	[61]	-16.02	0.160	209	0.67
NL3	[62]	-16.24	0.148	272	0.59
NL-Z2	[63]	-16.07	0.151	172	0.58
PC-F1	[41]	-16.17	0.151	270	0.61
NL-BA	[64]	-16.19	0.150	248	0.60

For study of surface properties there was developed semi-infinite nuclear matter extension of the models, for example, in relativistic mean-field framework [65]. Key properties of such a matter are the surface and asymmetry coefficients and the surface thickness.

A particular attention has to be paid to the pairing gap and odd-even staggering of masses. The unpaired nucleon contribution is not half of a pair, on top of it, it also breaks intrinsic time-reversal invariance. Thus all other nucleons rearrange themselves, which adds a contribution from the mean-field to odd-even staggering [66]. There are some difficulties arising from the fact that disentangling of the mean-field and pairing contributions is not simple. Additionally, also above-mentioned correlations can be expected to be different for odd and even nuclei. Pairing correlations give significant corrections to several observables which can be used to determine the parameters of more complicated pairing interactions.

One can see that there are many possibilities for a choice of an effective force phenomenological input. The mostly used parametrizations with these inputs are listed in Tab. 2 and Tab. 3. Generally, the earlier parametrization used the less data taken into account. For SkI1-5, NL-Z2 there is listed full set of input data, while its fitting strategy was initially used for Z_σ, NL1, NL-Z and PL-40 with smaller data set.

There are some differences between relativistic and nonrelativistic models that are caused by relativistic kinematics, as in the energy per baryon, saturation density value, effective mass ratio and also incompressibility modulus. They are larger than estimated extrapolation errors from least-squares method, and have to be fully understood yet. They cannot be caused by a finite range of interactions, as it is seen from point-coupled model PC-F1 results (see Tab. 1).

The prediction of the parametrizations for neutron matter equation of state is shown in Fig. 2. Skyrme interactions give a wide window of predictions, nevertheless, SLy6 interactions are well accommodated for neutron data. Relativistic mean-field interactions are unable to fit variational many-body calculations, and

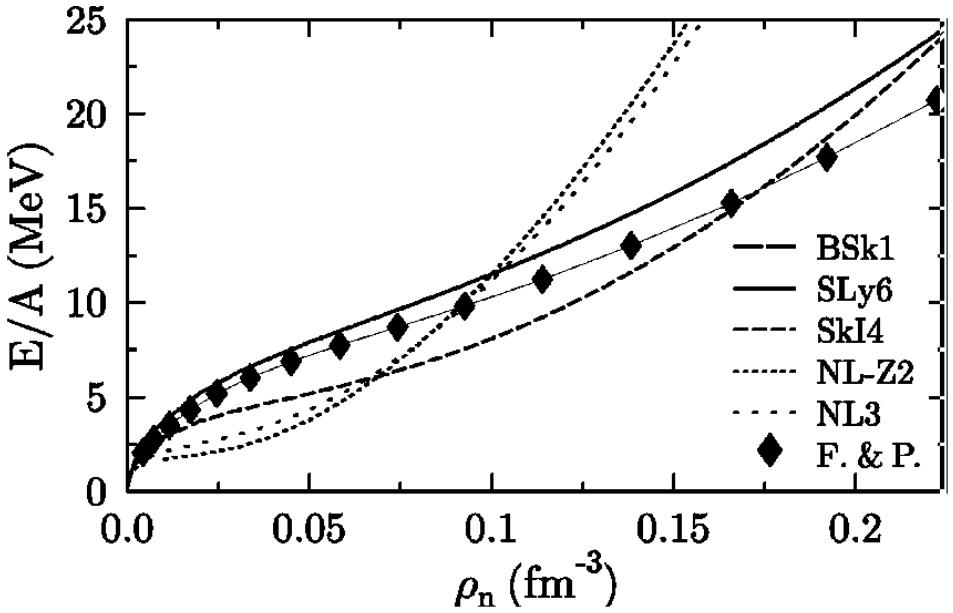

Figure 2: Energy per particle in neutron matter calculated with several parametrizations from Tab. 2 and Tab. 3. Filled lozenges connected with a thin solid line represent results from a variational many-body calculations [54] which are frequently used as reference data for neutron matter.

extensions are inevitable.

The Gogny force, the Skyrme energy functional as well as the relativistic mean-field parametrizations are able to describe nuclear bulk properties very satisfactorily. Additionally, also excitation properties such as fission, vibrational states, rotations and giant resonances can also be very well accommodated. However, differences among the models and some problems arise in some observables and in an extrapolation to exotic regions. For more detailed information about weaknesses and open problems in description of finite nuclei and nuclear matter see, e.g., review [55].

To enclose this part of overview from slightly more general point of view of quantum hadrodynamics one can say that in concordance with original motivation of QHD development, the progress proceeds also towards its extrapolation to high baryon densities and temperatures. The predictive power of mean-field theories leans on expanding in ratios of field strengths to meson masses instead of fields

Table 2: Compilation of various observables considered for different parametrizations, as taken from Ref. [55]. E = binding energy, r = charge rms radius, R = charge diffraction radius, σ = charge surface thickness, δr^2 = isotopic shift of charge m.s. radius, r_n = neutron rms radius, INM = infinite nuclear matter (E_b = binding energy per nucleon at saturation density, ρ_B^{sat} = saturation baryon density, K_∞ = incompressibility, a_{sym} = symmetry energy, m_0^*/m = effective baryon mass ratio, κ_{TRK} = sum-rule enhancement factor).

Gogny D1, D1S [61]	
E, r:	^{16}O, ^{19}Zr
$l.\mathbf{s}$:	^{16}O(1p$_n$),1p$_p$
INM	equilibrium symmetric INM
Pairing:	even-odd E in Sn isotopes (quenched)
SI-SVI [56]	
E:	^{16}O,^{40}Ca,^{48}Ca,^{56}Ni,^{90}Zr,^{140}Ce,^{208}Pb
r:	^{16}O,^{40}Ca,^{48}Ca,^{56}Ni,^{90}Zr,^{140}Ce,^{208}Pb
$l.\mathbf{s}$:	^{16}O(1p$_n$),1p$_p$
INM:	additionally for SkM [69]
	K_∞, a_{sym} (resonances in ^{208}Pb),
INM	additionally for SkM* [57]
	surface energy (fission barriers)
SkP [58]	
E:	^{16}O, ^{208}Pb
$l.\mathbf{s}$:	differences E
INM:	E_b, ρ_B^{sat}, K_∞, a_{sym}, κ_{TRK}, m_0^*/m=1, $a_{sym}(\rho/2)$
Pairing:	average gaps
SLy1-10 [59]	
E:	^{16}O,^{40}Ca,^{48}Ca,^{56}Ni,^{78}Ni,^{132}Sn,^{208}Pb
r:	^{16}O,^{40}Ca,^{48}Ca,^{56}Ni,^{208}Pb
$l.\mathbf{s}$:	^{208}Pb(3p$_n$)
INM:	E_b, ρ_B^{sat}, K_∞, a_{sym}, κ_{TRK}, EOS$_{neut}$
SkI1-5 [27], NL-Z2 [63],	(NL-Z [35], PL-40 [70], NL1 [71], Z$_\sigma$ [72])
E:	^{16}O,^{40}Ca,^{48}Ca,^{56}Ni,^{58}Ni,^{88}Sr,^{90}Zr, ^{112}Sn,^{120}Sn,
	^{124}Sn,^{132}Sn,^{144}Gd,^{208}Pb,^{214}Pb
R:	^{16}O,^{40}Ca,^{48}Ca,^{58}Ni,^{88}Sr,^{90}Zr, ^{112}Sn,^{120}Sn,^{124}Sn,^{208}Pb
σ:	^{16}O,^{40}Ca,^{48}Ca,^{90}Zr,^{208}Pb
$l.\mathbf{s}$:	^{16}O(1p$_n$,1p$_p$) (only Skyrme HF)
δr^2:	^{214}Pb-^{208}Pb (only Skyrme HF)
INM:	κ_{TRK} (only Skyrme HF)

Table 3: Completion of the previous table. All notations are identical.

NL3 [62]	
E:	^{16}O,^{40}Ca,^{48}Ca,^{58}Ni,^{90}Zr, ^{116}Sn,^{124}Sn,^{132}Sn,^{208}Pb,^{214}Pb
r:	^{16}O,^{40}Ca,^{48}Ca,^{58}Ni,^{90}Zr, ^{116}Sn,^{124}Sn,^{208}Pb,^{214}Pb
r_n:	^{40}Ca,^{48}Ca,^{58}Ni,^{90}Zr,^{116}Sn, ^{124}Sn,^{208}Pb
INM:	E_b, ρ_B^{sat}, K_∞, a_{sym}

themselves which are too large. This is the reason of relative success of MFT and also its main limitation. Reliable description of transition of baryon matter to quark-gluon plasma (more generally examined in Ref. [67, 68]) is important, and has a direct connection to a wide range of phenomena - early universe matter, supernova explosions, high-energy heavy-ion collisions etc. Only neutron stars provide zero temperature nuclear matter (except protoneutron stars) while most of other processes require an extension to finite temperature. It is straightforward in MFT, since the hamiltonian is diagonal and the mean-field thermodynamic potential can be calculated exactly. An analysis of nuclear matter at finite temperature is performed in Ref. [73]. Incorporation of heavier baryons - hyperons - into finite nuclei calculations (in the MFT framework in, e.g., Ref. [74]) appears also interesting. The role of hyperons in the nuclear matter will be analyzed also in this work. Recently many works have explored modification of hadron masses in nuclear medium [75, 76], its influence on nuclear force [77] and on relativistic transport [78]. Kaon condensation was also studied in Ref. [79, 80]. One of QHD enhancements is also developing the theories where meson couples directly to quarks [81, 82]. The endeavor is to find a connection between quark-meson interaction and observed nucleon-meson coupling constants. Perspective way of the development in the recent years has been also a better understanding of nuclear matter with high isospin asymmetry, which is also one of the goals of this dissertation.

For detailed review of recent progress in QHD see e.g. [30, 83] and references

therein. More detailed view of closer to our work related topics will be given also in the next sections.

2.4 Experimental Facilities

Theoretical effort is inherently associated with experiments. Whenever innovative experimental techniques for accelerating and/or detecting particles have been developed, new and - quite often - unexpected features have shown up. In that respect it is of utmost importance for the nuclear physics community to develop new apparatus to explore atomic nuclei by heating the nucleus (temperature degree of freedom), by bringing angular momentum to the nucleus (extremely rapid rotating nuclei), by forming very proton- and neutron-rich nuclei (approaching and mapping the drip line regions), and, in general, by exposing the atomic nucleus to an external agent and studying its response. In all that topics the isovector part of effective interactions is of utmost importance.

The landscape of nuclear physics has been altered by several top facilities during the recent years. Better understanding of strong interactions at the partonic level is expected to be provided by high-energy nuclear physics facilities: RHIC (Relativistic Heavy Ion Collider) [84] at Brookhaven national Laboratory that began operation in 2000, and CEBAF (Continuous Electron Beam Accelerator Facility) [85] at the Thomas Jefferson National Accelerator Laboratory. Nuclear physics is, however, not defined by a single frontier. Low-energy facilities continue to be an important part of the enterprise. They fall into two complementary types - the fast beam or in-flight method and the ISOL (Isotop Separation On-Line) or re-accelerated beam approach. Exploitation of the in-flight method is highly developed in the National Superconducting Cyclotron Laboratory at the Michigan State University [86]. In North America (TRIUMF - Canada's national Laboratory for Particle and Nuclear Physics [87], and Oak-Ridge National Laboratory [88]) similar activities in radioactive beam research are going on. Vigorous activity in these fields is seen also in Europe where several projects are running

- two new ISOL-based radioactive beam facilities have produced their first scientific results (SPIRAL at GANIL (Grand Accelerateur National D'Ions Lourds) [89] and REX-ISOLDE in CERN [90]). The community is preparing for the next generation of experiments like the International Accelerator for Beams of Ions and Antiprotons at GSI Darmstadt [91], and the European Isotope Separator On-Line (EURISOL) at GANIL. Furthermore, apart from the European effort in the second generation facilities, a new route towards combining the benefits of both the ISOL and in-flight techniques will be explored at RIA (Rare Isotope Accelerator) [92] in the US, and an in-flight facility called Radioactive Ion Beam Factory is proposed in Japan, where already valuable scientific results have been obtained at the RIKEN Research Accelerator Facility [93]. Facilities for the study of exotic nuceli are under construction also in Russia, China and India.

2.5 Astrophysical Observation Progress

Nuclear matter is a subject of study not only for nuclear physics but also for astrophysics. Several astrophysical objects and phenomena are directly connected to nuclear matter problems, like finite stages of stellar evolution (supernovae explosions, protoneutron stars and neutron stars) and the early universe. Several frequently used theoretical models of neutron star structure are illustrated in Fig. 3.

Experimental observations are continuously increasing in their precision and reliability. For example, currently about 1400 pulsars (rapidly rotating neutron stars) are known. Especially orbital observatories such as Hubble Space Telescope, the Chandra X-Ray observatory and the X-Ray Multi Mirror Mission allow us to obtain highly precise and reliable neutron star data. The gravitational mass of neutron star can be extracted directly from observations of X-ray binaries and binary radio pulsar systems. This masses appear to be concentrated around 1.35 solar mass [94], however, some observations indicate higher masses, probably due to accreted matter [95]. When rotational frequencies of fast pulsars

are combined with mass data they can also provide constraint on the equation of state. The fastest pulsar observed has a period of 1.6 ms, however, observational methods are of pure sensitivity to millisecond pulsars, thus biasing the data to a considerable amount [96]. Next important property of a neutron star is its radius. Direct radius observation do not exists, nevertheless, undirect analyzes lead to radii around 10 km or less (e.g., [97]). Besides moment of inertia, also gravitational red shift offers a possibility of EOS constraint. Strong magnetic field of neutron stars, in extreme cases called magnetars [98], can also significantly affect a structure of compact star [99]. Finally, X-ray observatories like ASCA and ROSAT provide a detection of thermal photons from stellar surface where surface temperatures of stars are derived from measured flux and spectrum. Thus, it is possible to observe cooling ratio of neutron star that depends strongly on neutron star matter properties, mostly on proton fraction, an existence of Bose-Einstein condensates, or superfluidity occurence. From the most recent results follows that the brightest isolated neutron star RXH1856 analyzes indicate that there may be no need for considering of strange quark matter or hybrid hyperon-quark matter

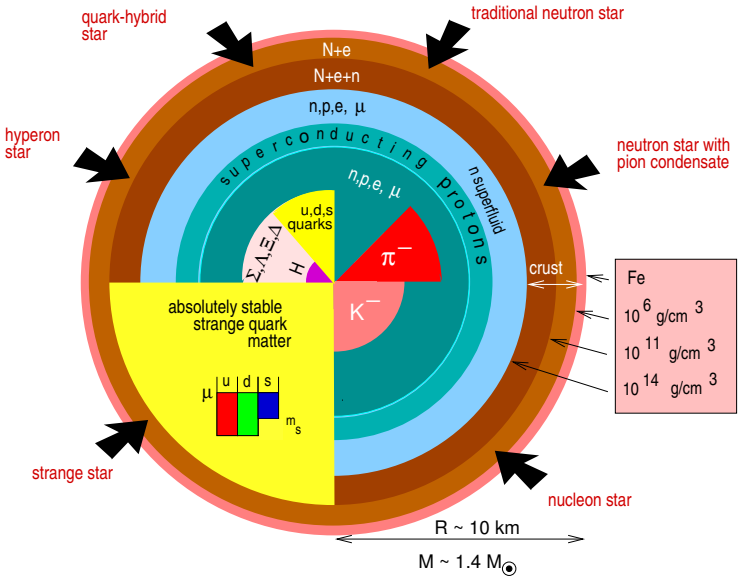

Figure 3: Illustration of neutron star structure described by several different theoretical models.

[100], and even at very high densities only hyperonic matter may occur, as it is also in this work assumed.

Thus, now one may be able to constrain the dense matter properties at the level unreachable before. From numerous studies of application of nuclear matter to neutron stars we can briefly name [101] in mean-field approach, [102] in Dirac-Brueckner-Hartree-Fock approach, and other [103]. More detailed recent review of nuclear and high-energy astrophysics is available in [104].

2.6 Strange Matter Physics

Since in the neutron star interior we expect densities several times of the nuclear saturation density, extrapolation of models to high density region is inevitable. Classical view of matter consisting of protons, neutrons and electrons is thus insufficient and more realistic composition is needed. At higher densities the K^--condensate [105], quark deconfinement [106] and/or hyperons [107] are possible to appear. We will discuss more closely the latter case.

When new particles in the cosmic ray experiments were discovered, they were entitled as "strange" due to their unusual long lifetimes of about 10^{-10} sec. The new quantum number "strangeness" has been introduced. While protons (uud) and neutrons (udd) consist of three quark in the quark picture interpretation, hyperons contain one strange quark (Λ hyperon (uds) and the triple of Σ hyperons (uus,uds,dds)), two strange quarks (Ξ hyperons (uss,dss)) or three strange quarks (Ω hyperon (sss)). After theoretical suggestion of hyperon appearance in high density nuclear matter [108] and hypernuclei [109] many works paid attention to them, e.g., [110, 111, 112, 113]. However, the strangeness is still largely unexplored degree of freedom. This is due to a lack of experimental data that are restricted to replacing one (at maximum two) neutrons by a strange Λ (or Σ) hyperon. There exist no experimental knowledge about behavior of more than two hyperons inside nuclei or nuclear matter. The difficulty is to create enough hyperons within hyperon decay time scale and bring them together with nucle-

ons to form any multi-hypernuclei. Another theoretical possibilities of stable hyperon systems are metastable exotic multi-hypernuclear objects (MEMO), or even states with more than three quarks. This speculative form of hypermatter, called strange quark matter or strangelets, could be possibly more bound than ^{56}Fe. Since this topic is beyond the scope of this work we will not discuss it in more detail, for further information see, e.g., [114].

2.6.1 Strange Hadronic Matter

In 1953 there were the first Λ hypernuclei in cosmic ray emulsion experiment observed [115]. The lightest one is ${}^{3}_{\Lambda}$H, a system of one proton, one neutron and one Λ. From other hypernuclei features it is interesting, for example, the existence of ${}^{9}_{\Lambda}$Be, where Λ stabilizes ^{8}Be which normally decays to two α particles. Similarly it works also in the case of ${}^{9}_{\Lambda}$Li and ${}^{9}_{\Lambda}$B. In the 70's systematical hypernuclei detection programs started at the AGS, CERN, in 80's it was joint also by KEK in Japan. These experimental effort led to a creation of hypernuclei shown in Fig. 4. Hypernuclei up to baryon number of A = 209 has been observed so far.

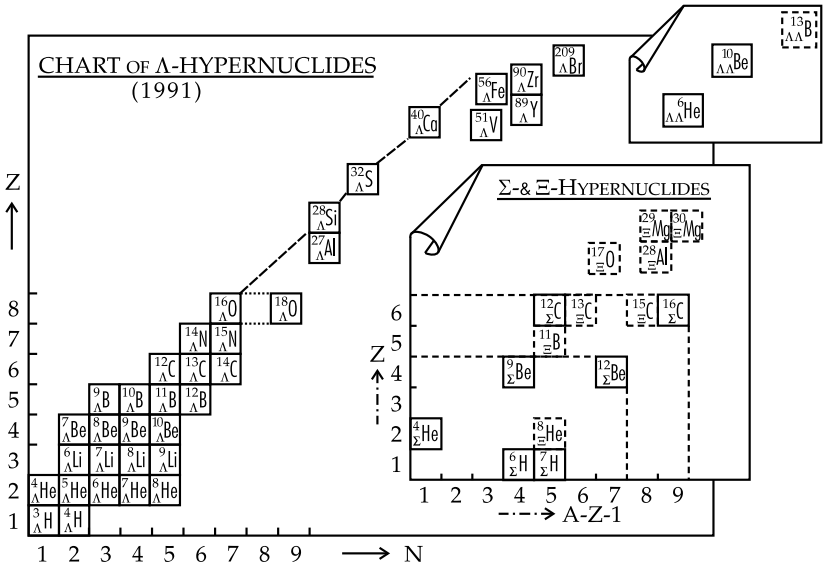

Figure 4: The chart of known Λ, Ξ and Σ hypernuclei as well as double Λ hypernuclei. Taken from [114].

The single particle binding energies from excited states to very deep lying states are capable to be extracted, thus opening the possibility to study deeply bound probes in nucleus over a wide range of mass number. The Λ-nucleon interaction is characteristic by no spin-orbit splitting experimental observation and due to an existence of several restrictions on its binding to nucleon it is relatively the best known hyperon-nucleon coupling [116]. Thus Λ seems to behave as a spinless neutron [117]. The potential depth of the Λ in nuclear matter derived from experimental data is $U_\Lambda^{(N)} \approx 30$ MeV. The observed trend of the single particle energy with the mass number is very well reproduced by relativistic mean-field models (e.g., [112]). Another measured quantity is the lifetime of hypernuclei. They decay weakly by an emission of a pion (mesonic decay channel, $\Lambda \to p + \pi^-$ and $\Lambda \to n + \pi^0$) like a free Λ or by nonmesonic decay in nuclear medium ($\Lambda + p \to n + p$ and $\Lambda + n \to n + n$). For heavier hypernuclei like ${}^{12}_{\Lambda}\mathrm{C}$ the mesonic channel is negligible. Finally, the lifetime of hypernuclei is determined to be at the order of 10^{-10} s even for $A \approx 200$ [118], and is thus close to the lifetime of a free Λ. There exists only vague information about Σ and Ξ hypernuclei. The existence of Σ hypernuclear systems is not experimentally clearly proved. Some recent information indicates that due to repulsive potential depth of Σ in nuclear medium there could exist no stable Σ hypernuclear state [119]. However, the Ξ hypernuclei was found short after the first observation of Λ hypernucleus. The potential depth of Ξ calculated by relativistic mean field models gives a value of $U_\Xi^{(N)} \doteq 28$ MeV [120]. There exist only three double Λ hypernuclei - ${}^{6}_{\Lambda\Lambda}\mathrm{He}$, ${}^{10}_{\Lambda\Lambda}\mathrm{Be}$ and ${}^{13}_{\Lambda\Lambda}\mathrm{B}$. Therefore, our knowledge of hyperon-hyperon interaction is very poor. However, it seems to be much stronger than ΛN interaction [121] and about 3/4 of the NN interaction, and thus it has to be taken into account in hyperon-rich systems. In this field a continuing activity is constantly developed [122]. Deeper overview of hyperon problematics one can find in Ref. [123, 124].

2.6.2 Strange Matter in Neutron Stars

Neutron star matter is not solely composed of neutrons but at higher energies it consists also of a considerable amount of protons as well as hyperons. Thus incorporation of strangeness into models has a significant influence on its description.

Neutron star properties partially depend on the composition of baryonic matter or on the abundance of its constituents. Thus, analyzes of density dependence of particle populations in neutron star matter performed also in this work are a base for further calculation of properties of these objects. The first heavier baryons appearing are Σ^- hyperons, followed by Λs. Naturally also other hyperons can be created at higher densities, however, it depends on a central density of neutron star and on hyperon-nucleon couplings, both still being of uncertain value. In any case the abundance of particular heavier components seems to have a weak effect on bulk properties of hyperon matter [125, 126], due to a similar influence of heavier Ξ^- hyperon which the same as Λ feels an attractive potential [127].

Since a neutron star structure is not a topic of this work we will not discuss this problematics in detail, for more information see an overview [128].

3 Mean-Field Approach for Nuclear Matter

The study of nuclear matter - a hypothetical uniform infinite system of nucleons - has been an important part of the nuclear physics for several decades. This is a starting point for describing more complicated and realistic phenomena not only in nuclear physics (structure and properties of finite nuclei, dynamics of heavy-ion collisions) but also in astrophysics (structure and evolution of neutron stars).

We will describe framework of the relativistic mean-field theory. By reason that new experimental facilities have been developed by continual improvement of particle accelerators, it is available nowadays to measure properties of exotic nuclei with high isospin asymmetry. Additionally, increasingly more precise observations and measurements of properties of neutron stars and supernovae have been carried out. This naturally brings a need for better description of isospin degree of freedom which can be done by enhancing the isovector meson sector. The isovector scalar δ meson [33] and vector cross interaction (VCI) [34] were included into MFT for this purpose.

3.1 Asymmetric Nuclear Matter

The starting point of the model is lagrangian density that introduces nucleon field ψ, isoscalar scalar meson field σ, isoscalar vector meson field $\boldsymbol{\omega}$, isovector vector meson field $\boldsymbol{\rho}$ and isovector scalar meson field δ (see Tab. 4)[1], and takes a form

$$\begin{aligned}\mathcal{L}(\psi,\sigma,\boldsymbol{\omega},\boldsymbol{\rho},\delta) = \bar{\psi}\left[\boldsymbol{\gamma}_\mu(i\partial^\mu - g_\omega\boldsymbol{\omega}^\mu - (M - g_\sigma\sigma)\right]\psi \\ +\tfrac{1}{2}(\partial_\mu\sigma\partial^\mu\sigma - m_\sigma^2\sigma^2) - \tfrac{1}{4}\boldsymbol{\omega}_{\mu\nu}\boldsymbol{\omega}^{\mu\nu} + \tfrac{1}{2}m_\omega^2\boldsymbol{\omega}_\mu\boldsymbol{\omega}^\mu \\ -\tfrac{1}{3}b_\sigma M(g_\sigma\sigma)^3 - \tfrac{1}{4}c_\sigma(g_\sigma\sigma)^4 + \tfrac{1}{4}c_\omega(g_\omega^2\boldsymbol{\omega}_\mu\boldsymbol{\omega}^\mu)^2 \\ +\tfrac{1}{2}(\partial_\mu\delta\partial^\mu\delta - m_\delta^2\delta^2) + \tfrac{1}{2}m_\rho^2\boldsymbol{\rho}_\mu.\boldsymbol{\rho}^\mu - \tfrac{1}{4}\boldsymbol{\rho}_{\mu\nu}.\boldsymbol{\rho}^{\mu\nu}\end{aligned}$$

[1] pion field does not contribute because it is pseudoscalar, and nuclear matter is parity invariant

$$+\tfrac{1}{2}\Lambda_V(g_\rho^2\boldsymbol{\rho_\mu}.\boldsymbol{\rho}^\mu)(g_\omega^2\boldsymbol{\omega}_\mu\boldsymbol{\omega}^\mu)$$
$$-g_\rho\boldsymbol{\rho}_\mu\bar{\psi}\gamma^\mu\boldsymbol{\tau}\psi + g_\delta\delta\bar{\psi}\boldsymbol{\tau}\psi \ , \tag{1}$$

where antisymmetric field tensors are given by

$$\boldsymbol{\omega}_{\mu\nu} \equiv \partial_\nu\boldsymbol{\omega}_\mu - \partial_\mu\boldsymbol{\omega}_\nu \ ,$$
$$\boldsymbol{\rho}_{\mu\nu} \equiv \partial_\nu\boldsymbol{\rho}_\mu - \partial_\mu\boldsymbol{\rho}_\nu \ ,$$

and the symbols used have their usual meaning [30]. The parameters entering the lagrangian are M that denotes the nucleon rest mass whereas m_σ, m_ω, m_ϱ, and m_δ are masses assigned to the mesons. The first term together with the last two ones describe interaction of isoscalar and isovector mesons with nucleons where the strength of these interactions is determined by dimensionless coupling constants g_σ, g_ω, g_ϱ and g_δ. Three terms in the third line represent cubic and quartic scalar self-interactions [129] and quartic vector self-couplings[2] [32, 130], the strength of which is also given by dimensionless self-interaction coupling constants b_σ, c_σ and c_ω. The second and fourth lines represent free (noninteracting) lagrangian for all mesons, and the fifth line realizes cross interaction between ω and ρ mesons[3] characterized by cross coupling constant Λ_V [34].

The constraint of stationarity of action for variations of arbitrary physical field Φ

$$\delta\int_{t_1}^{t^2} dt\int d^3x\,\mathcal{L}(\vec{x},t) = 0 \tag{2}$$

leads to the well-known Euler-Lagrange field equations

[2] cubic vector self-interactions are not possible due to parity conservation law. Initially, we have also incorporated isovector vector ρ meson self-interactions, however, its too large value indicates that physically it is not suitable degree of freedom. This effective parameter would improperly represent several physically undistinguished phenomena, and thus has not been used in the calculations.

[3] cross interaction between scalar σ and vector ρ mesons has also been tested, nevertheless, it turned out to have an equivalent effect as ω-ρ VCI and thus to be redundant if using fit of physical quantities considered.

Table 4: Masses and quantum numbers of particles considered (spin J, isospin I, strangeness S, hypercharge Y, third component of isospin I_3, and electric charge Q).

Particle	Mass [MeV]	J	I	S	Y	I_3	Q
N (p,n)	939	1/2	1/2	0	1	1/2,-1/2	1,0
σ	550	0	0	0	0	0	0
ω	783	1	0	0	0	0	0
ρ	770	1	1	0	0	1,0,-1	-1,0,1
δ	980	0	1	0	0	1,0,-1	-1,0,1

$$\frac{\partial \mathcal{L}}{\partial \Phi} - \partial^{\mu} \frac{\partial \mathcal{L}}{\partial(\partial^{\mu}\Phi)} = 0 \, . \tag{3}$$

Equations of motion follow after their application to the lagrangian (1). This produces the Dirac equation for nucleon field

$$[\boldsymbol{\gamma}_{\mu}(i\partial^{\mu} - g_{\omega}\boldsymbol{\omega}^{\mu} - g_{\rho}\boldsymbol{\rho}_{\mu}.\boldsymbol{\tau}) - (M - g_{\sigma}\sigma - g_{\delta}\delta\boldsymbol{\tau})]\,\psi = 0 \, . \tag{4}$$

Isoscalar meson fields σ,ω are then described by Klein-Gordon and Proca equations, respectively,

$$(\partial_{\mu}\partial^{\mu} + m_{\sigma}^2)\sigma = g_{\sigma}[\bar{\psi}\psi - b_{\sigma}M(g_{\sigma}\sigma)^2 - c_{\sigma}(g_{\sigma}\sigma)^3] \, , \tag{5}$$

$$\partial_{\mu}\boldsymbol{\omega}^{\mu\nu} + m_{\omega}^2\boldsymbol{\omega}^{\nu} = g_{\omega}[\bar{\psi}\gamma^{\nu}\psi - c_{\omega}g_{\omega}^3(\boldsymbol{\omega}_{\mu}\boldsymbol{\omega}^{\mu}\boldsymbol{\omega}^{\nu}) - g_{\rho}^2\boldsymbol{\rho}_{\boldsymbol{\mu}}.\boldsymbol{\rho}^{\mu}\Lambda_V g_{\omega}\boldsymbol{\omega}_{\mu}] \, . \tag{6}$$

Analogically, isovector ρ and δ meson fields read,

$$\partial_{\mu}\boldsymbol{\rho}^{\mu\nu} + m_{\rho}^2\boldsymbol{\rho}^{\nu} = g_{\rho}[\bar{\psi}\gamma^{\mu}\boldsymbol{\tau}\psi - g_{\rho}\boldsymbol{\rho}_{\mu}\Lambda_V g_{\omega}^2\boldsymbol{\omega}_{\mu}\boldsymbol{\omega}^{\mu}] \, , \tag{7}$$

$$(\partial_{\mu}\partial^{\mu} + m_{\delta}^2)\boldsymbol{\delta} = g_{\delta}\bar{\psi}\boldsymbol{\tau}\psi \, . \tag{8}$$

Due to the fact that these equations are nonlinear, nowadays there is known no suitable method to solve them and thus there is also no exact result. The

way to avoid this is to replace the operators of meson fields by their expectation values – the so-called mean-field approximation. The fields are thus treated as classical ones. Its reliability increases with rising baryon density. The second approximation introduced is the non-sea approximation which doesn't take account of the Dirac sea of negative energy states.

In this model we are dealing with static, homogenous, infinite nuclear matter that allows us to consider some other simplifications due to translational invariance and rotational symmetry of nuclear matter. This causes that the expectation values of space-like components of vector fields vanish and only zero components - ρ_0 and ω_0 - remain. In addition, rotational invariance around third axe of isospin space results in taking into account only the third component of isovector fields - $\rho^{(3)}$ and $\delta^{(3)}$ [5, 33]. The above-mentioned can formally be written as

$$\begin{aligned} \sigma &\longrightarrow \langle\sigma\rangle \equiv \bar{\sigma} \ , \\ \boldsymbol{\omega}_\mu &\longrightarrow \langle\boldsymbol{\omega}_\mu\rangle \equiv \delta_{\mu 0}\boldsymbol{\omega}_\mu = \bar{\omega}_0 \ , \\ \boldsymbol{\rho}_\mu &\longrightarrow \langle\boldsymbol{\rho}_\mu\rangle \equiv \bar{\rho}_0^{(3)} \ , \\ \delta &\longrightarrow \langle\delta\rangle \equiv \bar{\delta}^{(3)} \ . \end{aligned} \tag{9}$$

Having inserted the above simplifications the field equations are reduced and we can easily obtain potentials of both isoscalar meson fields

$$U_\sigma \equiv -g_\sigma\bar{\sigma} = -\frac{g_\sigma^2}{m_\sigma^2}[\rho_S - b_\sigma M(g_\sigma\bar{\sigma})^2 - c_\sigma(g_\sigma\bar{\sigma})^3] \ , \tag{10}$$

$$U_\omega \equiv g_\omega\bar{\omega}_0 = \frac{g_\omega^2}{m_\omega^2}[\rho_B - c_\omega(g_\omega\bar{\omega}_0)^3 - U_\rho^2\Lambda_V(g_\omega\bar{\omega}_0)] \ , \tag{11}$$

and isovector meson fields

$$U_\rho \equiv g_\rho\bar{\rho}_0^{(3)} = \frac{g_\rho^2}{m_\rho^2}[(2\frac{Z}{A} - 1)\rho_B - g_\rho\bar{\rho}_0^{(3)}\Lambda_V U_\omega^2] \ , \tag{12}$$

$$U_\delta \equiv -g_\delta\bar{\delta}^{(3)} = -\frac{g_\delta^2}{m_\delta^2}\bar{\psi}\tau_3\psi = \frac{g_\delta^2}{m_\delta^2}(\rho_n^S - \rho_p^S) \ , \tag{13}$$

where scalar density ρ_S is expressed as the sum of proton (p) and neutron (n) part

$$\rho_S = \left\langle \bar{\psi}\psi \right\rangle = \rho_p^S + \rho_n^S \,, \tag{14}$$

which are given by

$$\rho_i^S = \frac{2}{(2\pi)^3} \int_0^{k_i} d^3k \, \frac{M_i^*}{\left(\boldsymbol{k}^2 + M_i^{*2}\right)^{1/2}} \,, i = p, n \,. \tag{15}$$

In Eq. (15) k_i is nucleons' Fermi momentum and M_p^*, M_n^* denotes proton and neutron effective masses, respectively, which can be written as

$$M_p^* = M - g_\sigma \bar{\sigma} - g_\delta \bar{\delta}^{(3)} \,, \tag{16}$$

$$M_n^* = M - g_\sigma \bar{\sigma} + g_\delta \bar{\delta}^{(3)} \,. \tag{17}$$

One can see that condensed scalar σ meson field generates a shift of nucleon mass in consequence of which the nuclear matter is described as a system of pseudonucleons with masses M^* moving in classical fields $\bar{\sigma}$, $\bar{\omega}_0$ and $\bar{\rho}_0{}^{(3)}$ where, additionally, δ meson field is responsible for splitting of proton and neutron effective masses which is an important feature of δ meson influence on the nuclear matter saturation mechanism and its properties. The δ meson seemed to be an useful degree of freedom in describing of asymmetric nuclear matter, indicated by its influence on, e.g., stiffness of equation of state, slope and curvature of symmetry energy and properties of warm asymmetric nuclear matter [33, 131].

The solution requires to be performed self-consistently which can be clearly seen from Eqs. (10)-(17) where σ potential (10) must be solved using iterations.

The baryon density is given by

$$\rho_B = \left\langle \bar{\psi}\gamma^0\psi \right\rangle = \frac{4}{(2\pi)^3} \int_0^{k_F} d^3k = \frac{2}{3\pi^2} k_F^3 \,, \tag{18}$$

with k_F being an average Fermi momentum. It can be seen that scalar density (15) is less than baryon density due to term $M_i^*/(\boldsymbol{k}^2 + M_i^{*2})^{1/2}$ that causes reduction of the contribution of rapid moving nucleons to scalar source term. This mechanism is responsible for nuclear matter saturation in the mean field theory and essentially distinguishes relativistic models from nonrelativistic ones.

Cross coupling of the ω and ρ mesons requires also self-consistent calculation of Eqs. (11) and (12), with iterative procedure for ω potential.

By reason that δ field splits nucleon effective masses, the proton and neutron Fermi momenta will be also splitted, while they have to fulfil

$$\rho_B = \rho_p + \rho_n = \frac{2}{(2\pi)^3}\int_0^{k_p} d^3k + \frac{2}{(2\pi)^3}\int_0^{k_n} d^3k \ , \tag{19}$$

where k_p, k_n are Fermi momenta of protons and neutrons, respectively. The different value of Fermi momenta has consequences for the transport properties of asymmetric nuclear matter.

To obtain formula for energy density of nuclear matter it is essential to have cognizance of the energy tensor, in continuum mechanics defined [132] as

$$T_{\mu\nu} = -g_{\mu\nu}\mathcal{L} + \frac{\partial\Phi_i}{\partial \boldsymbol{x}^\nu}\frac{\partial\mathcal{L}}{\partial(\partial\Phi_i/\partial \boldsymbol{x}_\mu)} \ , \tag{20}$$

where Φ_i generally denotes physical fields. The energy density of such a system is the zero component of the energy tensor $\varepsilon = \langle T_{00}\rangle$.

To obtain relation for energy density, we start from Eq. (20)

$$\begin{aligned} T_{\mu\nu}^{\mathrm{MFT}} = -g_{\mu\nu}\Big(&-\frac{1}{2}m_\sigma^2\bar{\sigma} + \frac{1}{2}m_\omega^2\bar{\omega}_0^2 - \frac{1}{2}m_\delta^2\bar{\delta}^{(3)\,2} + \frac{1}{2}m_\rho^2\bar{\rho}_0^{(3)\,2} \\ &-\frac{1}{3}b_\sigma M(g_\sigma\bar{\sigma})^3 - \frac{1}{4}c_\sigma(g_\sigma\bar{\sigma})^4 + \frac{1}{4}c_\omega(g_\omega\bar{\omega}_0)^4\Big) \qquad (21) \\ &+\frac{1}{2}\Lambda_V(g_\rho\bar{\rho}_0^{(3)})^2(g_\omega\bar{\omega}_0)^2 + i\bar{\psi}\gamma_\mu\partial_\nu\psi \ . \qquad (22) \end{aligned}$$

The energy density being zero component of this tensor takes a form

$$\begin{aligned}\varepsilon = T_{00}^{\mathrm{MFT}} &= \frac{1}{2}m_\sigma^2\bar{\sigma}^2 - \frac{1}{2}m_\omega^2\bar{\omega}_0^2 + \frac{1}{2}m_\delta^2\bar{\delta}^{(3)\,2} - \frac{1}{2}m_\rho^2\bar{\rho}_0^{(3)\,2} \\ &+\frac{1}{3}b_\sigma M(g_\sigma\bar{\sigma})^3 + \frac{1}{4}c_\sigma(g_\sigma\bar{\sigma})^4 - \frac{1}{4}c_\omega(g_\omega\bar{\omega}_0)^4 \\ &-\frac{1}{2}\Lambda_V(g_\rho\bar{\rho}_0^{(3)})^2(g_\omega\bar{\omega}_0)^2 + i\bar{\psi}\gamma_0\partial_0\psi\ ,\end{aligned} \tag{23}$$

from which using Dirac equation (4) follows

$$\begin{aligned}\varepsilon = \psi^+ &\left[-i\boldsymbol{\alpha}.\boldsymbol{\nabla} + \beta M_{N,P}^* + g_\omega\bar{\omega}_0 + g_\rho\rho_0^{(3)}\tau_3\right]\psi \\ &+\frac{1}{2}m_\sigma^2\bar{\sigma}^2 - \frac{1}{2}m_\omega^2\bar{\omega}_0^2 + \frac{1}{2}m_\delta^2\bar{\delta}^{(3)\,2} - \frac{1}{2}m_\rho^2\bar{\rho}_0^{(3)\,2} \\ &+\frac{1}{3}b_\sigma M(g_\sigma\bar{\sigma})^3 + \frac{1}{4}c_\sigma(g_\sigma\bar{\sigma})^4 - \frac{1}{4}c_\omega(g_\omega\bar{\omega}_0)^4 \\ &-\frac{1}{2}\Lambda_V(g_\rho\bar{\rho}_0^{(3)})^2(g_\omega\bar{\omega}_0)^2\ .\end{aligned} \tag{24}$$

After further manipulation for nucleon contribution to energy density we obtain

$$\varepsilon_{\mathrm{NUC}} = \frac{2}{(2\pi)^3}\left[\int_0^{k_p} d^3k\,\sqrt{\boldsymbol{k}^2 + M_p^{*2}} + \int_0^{k_n} d^3k\,\sqrt{\boldsymbol{k}^2 + M_n^{*2}}\right]\ , \tag{25}$$

For ω meson field contribution we have

$$\varepsilon_\omega = U_\omega\rho_B - \frac{1}{2}\frac{m_\omega^2}{g_\omega^2}U_\omega^2 - \frac{1}{4}c_\omega U_\omega^4\ . \tag{26}$$

Field of σ meson contributes by

$$\varepsilon_\sigma = \frac{1}{2}\frac{m_\sigma^2}{g_\sigma^2}(g_\sigma\bar{\sigma})^2 + \frac{1}{3}b_\sigma M(g_\sigma\bar{\sigma})^3 + \frac{1}{4}c_\sigma(g_\sigma\bar{\sigma})^4\ . \tag{27}$$

Isovector vector component of the energy density has a form

$$\varepsilon_\rho = U_\rho(2\frac{\rho_p}{\rho_B} - 1)\rho_B - \frac{1}{2}\frac{m_\rho^2}{g_\rho^2}U_\rho^2\ . \tag{28}$$

Energy density induced by δ meson field is

$$\varepsilon_\delta = \frac{1}{2} m_\delta^2 \bar{\delta}^{(3)\,2} = \frac{1}{8} \frac{m_\delta^2}{g_\delta^2} (M_n^* - M_p^*)^2 \,, \tag{29}$$

and, finally, vector cross interaction is represented as

$$\varepsilon_{\omega-\rho} = -\frac{1}{2} U_\rho^2 \Lambda_V U_\omega^2 \,. \tag{30}$$

Thus, after expression of integrals (25) the complete formula for the energy density in the frame of the model considered will be

$$\begin{aligned}
\varepsilon = \varepsilon_p + \varepsilon_n + \varepsilon_\sigma + \varepsilon_\omega + \varepsilon_\rho + \varepsilon_\delta + \varepsilon_{\omega-\rho} \\
= \tfrac{1}{\pi^2} \left[\tfrac{1}{4} k_p E_p^{*3} - \tfrac{1}{8} M_p^{*2} k_p E_p^* - \tfrac{1}{8} M_p^{*4} \ln \left(\tfrac{|k_p + E_p^*|}{M_p} \right) \right] \\
+ \tfrac{1}{\pi^2} \left[\tfrac{1}{4} k_n E_n^{*3} - \tfrac{1}{8} M_n^{*2} k_n E_n^* - \tfrac{1}{8} M_n^{*4} \ln \left(\tfrac{|k_n + E_n^*|}{M_n} \right) \right] \\
+ U_\omega \rho_B - \tfrac{1}{2} \tfrac{m_\omega^2}{g_\omega^2} U_\omega^2 - \tfrac{1}{4} c_\omega U_\omega^4 \\
+ \tfrac{1}{2} \tfrac{m_\sigma^2}{g_\sigma^2} \left(M - \tfrac{M_p^* + M_n^*}{2} \right)^2 + \tfrac{1}{3} b_\sigma M \left(M - \tfrac{M_p^* + M_n^*}{2} \right)^3 + \tfrac{1}{4} c_\sigma \left(M - \tfrac{M_p^* + M_n^*}{2} \right)^4 \\
+ U_\rho (2 \tfrac{\rho_p}{\rho_B} - 1) \rho_B - \tfrac{1}{2} \tfrac{m_\rho^2}{g_\rho^2} U_\rho^2 + \tfrac{1}{8} \tfrac{m_\delta^2}{g_\delta^2} (M_n^* - M_p^*)^2 - \tfrac{1}{2} U_\rho^2 \Lambda_V U_\omega^2 \,,
\end{aligned} \tag{31}$$

where E_p^*,E_n^* are proton and neutron effective energies, respectively,

$$E_p^* = \sqrt{k_p^2 + M_p^{*2}} \,, \tag{32}$$

$$E_n^* = \sqrt{k_n^2 + M_n^{*2}} \,. \tag{33}$$

Finally, the binding energy per nucleon is related to energy density by

$$E_b = \frac{\varepsilon}{\rho_B} - M \,. \tag{34}$$

The energy density per nucleon is a starting quantity for further properties of nuclear matter. Incompressibility is given as its second derivative with respect to baryon density, at the saturation point

$$K = 9\left[\rho^2 \frac{\partial^2}{\partial \rho^2}(\frac{\varepsilon}{\rho_B})\right]_{\rho=\rho_0} . \tag{35}$$

Symmetry energy of nuclear matter is defined as the second derivative of binding energy per nucleon (denoted as S_2) with respect to the asymmetry parameter $\alpha = (\rho_p - \rho_n)/(\rho_p + \rho_n)$, fulfilling equation

$$\varepsilon(\rho, \alpha) = \varepsilon(\rho, 0) + S_2(\rho)\alpha^2 + S_4(\rho)\alpha^4, \tag{36}$$

with S_2 and S_4 defined as

$$S_2 = \frac{1}{2}\left[\frac{\partial^2 \varepsilon(\rho,\alpha)}{\partial \alpha^2}\right]_{\alpha=0} , \tag{37}$$

$$S_4 = \frac{1}{24}\left[\frac{\partial^4 \varepsilon(\rho,\alpha)}{\partial \alpha^4}\right]_{\alpha=0} . \tag{38}$$

Symmetry energy value S_2 at the saturation density is of special importance, often denoted as symmetry energy parameter a_4.

3.2 Hyperons

In this subsection we will introduce an additional degree of freedom - strangeness - in the mean-field framework. Mathematically it is straightforward. Lagrangian (1) is enriched by additional terms of the following form

$$\begin{gathered}
\mathcal{L}(\psi_{B,e^-,\mu^-}, \sigma, \boldsymbol{\omega}, \boldsymbol{\rho}, \delta, \sigma^*, \boldsymbol{\phi}) = \mathcal{L}(\psi_{p,n}, \sigma, \boldsymbol{\omega}, \boldsymbol{\rho}, \delta) \\
+ \textstyle\sum_Y \bar{\psi}_Y [\gamma_\mu (i\partial^\mu - g_{\omega Y}\boldsymbol{\omega}^\mu - g_{\rho Y}\boldsymbol{\rho}_\mu \bar{\psi}\gamma^\mu \boldsymbol{\tau} - g_{\phi Y}\boldsymbol{\phi}^\mu) \\
-(M - g_{\sigma Y}\sigma - g_{\delta Y}\delta\bar{\psi}\boldsymbol{\tau}\psi - g_{\sigma^* Y}\sigma^*)]\psi_Y \\
+\tfrac{1}{2}(\partial_\mu \sigma^* \partial^\mu \sigma^* - m_{\sigma^*}^2 \sigma^{*2}) + \tfrac{1}{2} m_\phi^2 \boldsymbol{\phi}_\mu \boldsymbol{\phi}^\mu - \tfrac{1}{4}\boldsymbol{\phi}_{\mu\nu}\boldsymbol{\phi}^{\mu\nu} \\
+ \textstyle\sum_{e,\mu} \bar{\psi}_{e,\mu}(i\gamma_\mu \partial^\mu - m_{e,\mu})\psi_{e,\mu} ,
\end{gathered} \tag{39}$$

where antisymmetric field tensor is given by

$$\boldsymbol{\phi}_{\mu\nu} \equiv \partial_\nu \boldsymbol{\phi}_\mu - \partial_\mu \boldsymbol{\phi}_\nu \ , \tag{40}$$

and the symbols used have the same meaning as in the first section. Y stands for additional hyperon degrees of freedom, the interaction terms of hyperons have the same form as for nucleons, differing only in coupling constants. New feature of this lagrangian is incorporation of two additional mesons - (hidden) strange scalar σ^* and vector $\boldsymbol{\phi}$ meson. These mesons are responsible for intermediation of the strong interaction between hyperons that contain strange quarks, thus simulating experimentally observed strong hyperon-hyperon interaction which is the reason for their inclusion. Couplings of these mesons to nucleons are zero as the nucleon does not contain any strange quarks. Formally, these new mesons are represented by interaction lagrangian where strength of baryon-meson interaction is determined by dimensionless coupling constants g_{σ^*}, g_ϕ; and correspondent non-interaction lagrangian, m_{σ^*}, m_ϕ being strange meson masses. Since we study the hyperon matter in β equilibrium, naturally also leptons appear which are treated as non-interacting free Fermi gas, represented by the last lagrangian term. These particles' masses and quantum numbers are listed in Tab. 5.

Table 5: Masses and quantum numbers of additional particles considered.

Particle	Mass [MeV]	J	I	S	Y	I_3	Q
Λ^0	1116	1/2	0	-1	0	0	0
Σ^-	1193	1/2	1	-1	0	-1	-1
e^-	0.511	1/2	0	0	0	0	-1
μ^-	105.65	1/2	0	0	0	0	-1
σ^*	975	0	0	0	0	0	0
ϕ	1020	1	0	0	0	0	0

Coupling constants of hyperons to vector and isovector mesons as well as vector strange mesons are derived from the quark model and are of the following form [120]:

$$\begin{aligned} \tfrac{1}{3}g_{\omega N} = \tfrac{1}{2}g_{\omega\Lambda} = \tfrac{1}{2}g_{\omega\Sigma}\ , \\ g_{\rho N} = \tfrac{1}{2}g_{\rho\Sigma}\ \ ,\ \ g_{\rho\Lambda} = 0\ , \\ g_{\delta N} = \tfrac{1}{2}g_{\delta\Sigma}\ \ ,\ \ g_{\delta\Lambda} = 0\ , \\ g_{\phi\Lambda} = g_{\phi\Sigma} = -\tfrac{\sqrt{2}}{3}g_{\omega N}\ \ ,\ \ g_{\phi N} = 0\ . \end{aligned} \tag{41}$$

Remaining couplings of hyperons to scalar mesons are adjusted to reproduce hypernuclei potentials in saturated nuclear matter [120]

$$U_{\Lambda}^{(N)} = U_{\Sigma}^{(N)} = -30\ \text{MeV}\ . \tag{42}$$

A recent analysis [133] shows that Σ^- can feel repulsion in nuclear matter, thus leading to strong suppression of its abundance in β stable hyperon matter. However, for our purposes it is of little importance because despite this fact it has minor effect on bulk hyperon matter properties as was shown in Ref. [125]. The matter is dominated by nucleons up to high densities where universal short-range forces are expected to take precedence over the specific baryon identities [126].

Finally, the hyperon couplings to scalar strange mesons are fixed by potential well of Λ-hyperon in Λ-hyperonic matter deduced from double-hypernuclear data [120]

$$U_{\Lambda}^{(\Lambda)} = -20\ \text{MeV}\ . \tag{43}$$

All baryons fulfill the Dirac equation

$$\sum_B [\boldsymbol{\gamma}_\mu(i\partial^\mu - g_\omega\boldsymbol{\omega}^\mu - g_\rho\boldsymbol{\rho}_\mu.\boldsymbol{\tau} - g_{\phi B}\boldsymbol{\phi}^\mu) - (M - g_\sigma\sigma - g_\delta\delta\boldsymbol{\tau} - g_{\sigma^* B}\sigma^*)]\psi_B = 0\ . \tag{44}$$

Original isoscalar σ, ω, and isovector δ, ρ equations of motion do not change significantly, and two equation for new mesons are added, having form of additional Klein-Gordon and Proca equations, respectively,

$$(\partial_\mu\partial^\mu + m_\sigma^2)\sigma = g_\sigma\Big[\sum_B \frac{g_{\sigma B}}{g_\sigma}\rho_B^S - b_\sigma M(g_\sigma\sigma)^2 - c_\sigma(g_\sigma\sigma)^3\Big] , \tag{45}$$

$$\partial_\mu\boldsymbol{\omega}^{\mu\nu} + m_\omega^2\boldsymbol{\omega}^\nu = g_\omega\Big[\sum_B \frac{g_{\omega B}}{g_\omega}\rho_B^B - c_\omega g_\omega^3(\boldsymbol{\omega}_\mu\boldsymbol{\omega}^\mu\boldsymbol{\omega}^\nu) - g_\rho^2\boldsymbol{\rho}_\mu.\boldsymbol{\rho}^\mu\Lambda_V g_\omega\boldsymbol{\omega}_\mu\Big] , \tag{46}$$

$$\partial_\mu\boldsymbol{\rho}^{\mu\nu} + m_\rho^2\boldsymbol{\rho}^\nu = g_\rho\Big[\sum_B \frac{g_{\rho B}}{g_\rho}\rho_B^B\boldsymbol{\tau} - g_\rho\boldsymbol{\rho}_\mu\Lambda_V g_\omega^2\boldsymbol{\omega}_\mu\boldsymbol{\omega}^\mu\Big] , \tag{47}$$

$$(\partial_\mu\partial^\mu + m_\delta^2)\delta = g_\delta\sum_B \frac{g_{\delta B}}{g_\delta}\rho_B^S\boldsymbol{\tau} , \tag{48}$$

$$(\partial_\mu\partial^\mu + m_{\sigma^*}^2)\sigma^* = g_{\sigma^*\Lambda}\sum_B \frac{g_{\sigma^* B}}{g_{\sigma^*\Lambda}}\rho_B^S , \tag{49}$$

$$\partial_\mu\boldsymbol{\phi}^{\mu\nu} + m_\phi^2\boldsymbol{\phi}^\nu = g_{\phi\Lambda}\sum_B \frac{g_{\phi B}}{g_{\phi\Lambda}}\rho_B^B . \tag{50}$$

The mean-field replacement of meson field operators by their expectation values can be in addition to Eq. (9) written as

$$\begin{aligned} \sigma^* &\longrightarrow \langle\sigma^*\rangle \equiv \bar{\sigma^*} , \\ \boldsymbol{\phi}_\mu &\longrightarrow \langle\boldsymbol{\phi}_\mu\rangle \equiv \delta_{\mu 0}\boldsymbol{\phi}_\mu = \bar{\phi}_0 . \end{aligned} \tag{51}$$

After reducing of equation of motion meson field potentials follow directly:

$$U_\sigma \equiv -g_\sigma\bar{\sigma} = -\frac{g_\sigma^2}{m_\sigma^2}[\sum_B \frac{g_{\sigma B}}{g_\sigma}\rho_B^S - b_\sigma M(g_\sigma\bar{\sigma})^2 - c_\sigma(g_\sigma\bar{\sigma})^3] , \tag{52}$$

$$U_\omega \equiv g_\omega\bar{\omega}_0 = \frac{g_\omega^2}{m_\omega^2}[\sum_B \frac{g_{\omega B}}{g_\omega}\rho_B^B - c_\omega(g_\omega\bar{\omega}_0)^3 - U_\rho^2\Lambda_V(g_\omega\bar{\omega}_0)] , \tag{53}$$

$$U_\rho \equiv g_\rho\bar{\rho}_0^{(3)} = \frac{g_\rho^2}{m_\rho^2}[\sum_B \frac{g_{\rho B}}{g_\rho}\rho_B^B\tau_{3B} - g_\rho\bar{\rho}_0^{(3)}\Lambda_V U_\omega^2] , \tag{54}$$

$$U_\delta \equiv -g_\delta\bar{\delta}^{(3)} = -\frac{g_\delta^2}{m_\delta^2}\sum_B \frac{g_{\delta B}}{g_\delta}(\rho_B^S\tau_{3B}) , \tag{55}$$

$$U_{\sigma^*} \equiv -g_{\sigma^*\Lambda}\bar{\sigma^*} = -\frac{g_{\sigma^*\Lambda}^2}{m_{\sigma^*}^2}\sum_B \frac{g_{\sigma^* B}}{g_{\sigma^*\Lambda}}\rho_B^S , \tag{56}$$

$$U_\phi \equiv g_{\phi\Lambda}\bar{\phi}_0 = \frac{g_{\phi\Lambda}^2}{m_\phi^2}\sum_B \frac{g_{\phi B}}{g_{\phi\Lambda}}\rho_B^B , \tag{57}$$

where $\tau_{3p} = 1, \tau_{3n,\Sigma^-} = -1, \tau_{3\Lambda^0} = 0$ are isospin projections for baryons. Scalar density ρ_S is expressed as the sum of baryon ($B = p, n, \Lambda^0, \Sigma^-$) contributions that, in comparison with Eq. (14), can be written more generally as

$$\rho_B^S = \frac{2J_B+1}{(2\pi)^3}\int_0^{k_B} d^3k\, \frac{M_B^*}{(\boldsymbol{k}^2 + {M_B^*}^2)^{1/2}} \ . \tag{58}$$

where k_B is baryons' Fermi momentum, $(2J_B + 1)$ corresponds to baryon spin degeneration factor and M_B^* denotes baryon effective masses that can be written as

$$M_B^* = M - g_{\sigma B}\bar{\sigma} - g_{\delta B}\bar{\delta}^3\tau_{3B} - g_{\sigma^* B}\bar{\sigma^*} \ . \tag{59}$$

Not only condensed scalar σ and δ fields as in pure nucleonic matter (see Eq. (17)) but, additionally, also σ^* meson fields generate a shift of baryon masses. Note that while σ meson shifts all the baryon masses (even with different strength for nucleons and hyperons), δ meson field is responsible for splitting of effective masses of baryons with non-zero isospin. Additionally, due to no interaction of strange mesons with nucleons, σ^* meson shifts only hyperon masses.

Total baryon density is given by

$$\rho_B = \sum_B \rho_B^B = \sum_B \frac{2J_B+1}{(2\pi)^3}\int_0^{k_B} d^3k = \sum_B \frac{k_B^3}{3\pi^2} \ . \tag{60}$$

The momentum-energy tensor (20) applied to lagrangian (39) after some algebra gives modified energy density per baryon

$$\begin{gathered}
\varepsilon = \varepsilon_{p,n,\Sigma^-,\Lambda^0} + \varepsilon_{\sigma,\omega,\rho,\delta,\sigma^*,\phi} + \varepsilon_{e^-,\mu^-} = \\
\textstyle\sum_B \frac{1}{\pi^2}\left[\frac{1}{4}k_B {E_B^*}^3 - \frac{1}{8}{M_B^*}^2 k_B E_B^* - \frac{1}{8}{M_B^*}^4 \ln\left(\frac{|k_B+E_B^*|}{M_B}\right)\right] \\
+\textstyle\sum_{e,\mu}\frac{1}{\pi^2}\left[\frac{1}{4}k_{e,\mu}E_{e,\mu}^3 - \frac{1}{8}m_{e,\mu}^2 k_{e,\mu}E_{e,\mu} - \frac{1}{8}m_{e,\mu}^4 \ln\left(\frac{|k_{e,\mu}+E_{e,\mu}|}{m_{e,\mu}}\right)\right] \\
+\textstyle\sum_B \frac{g_{\omega B}}{g_\omega}U_\omega\rho_B^B - \frac{1}{2}\frac{m_\omega^2}{g_\omega^2}U_\omega^2 - \frac{1}{4}c_\omega U_\omega^4 \\
+\textstyle\frac{1}{2}\frac{m_\sigma^2}{g_\sigma^2}(g_\sigma\bar{\sigma})^2 + \frac{1}{3}b_\sigma M(g_\sigma\bar{\sigma})^3 + \frac{1}{4}c_\sigma(g_\sigma\bar{\sigma})^4
\end{gathered}$$

$$+\sum_B \frac{g_{\rho B}}{g_\rho}\rho_B^B\tau_{3B} - \frac{1}{2}\frac{m_\rho^2}{g_\rho^2}U_\rho^2 + \frac{1}{2}\frac{m_\delta^2}{g_\delta^2}U_\delta^2 - \frac{1}{2}U_\rho^2\Lambda_V U_\omega^2$$
$$+\frac{1}{2}\frac{m_{\sigma^*}^2}{g_{\sigma^*\Lambda}^2}(g_{\sigma^*\Lambda}\bar{\sigma}^*)^2 + U_\phi\sum_B \frac{g_{\phi B}}{g_{\phi\Lambda}}\rho_B^B - \frac{1}{2}\frac{m_\phi^2}{g_{\phi\Lambda}^2}U_\phi^2 \ . \tag{61}$$

While we are considering β-stable nuclear matter consisting of nucleons, hyperons and leptons, the equilibrium conditions of chemical potentials defined as Fermi energy of particles at the top of Fermi sea must be fulfilled. Baryon chemical potential takes a form

$$\mu_B = g_{\omega B}\bar{\omega}_0 + g_{\rho B}\bar{\rho_0}^{(3)}\tau_{3B} + g_{\phi B}\bar{\phi}_0 + \sqrt{k_B^2 + {M_B^*}^2} \ , \tag{62}$$

and for leptons

$$\mu_{e,\mu} = \sqrt{k_{e,\mu}^2 + m_{e,\mu}^2} \ . \tag{63}$$

Generally, the chemical potential equilibrium conditions can be written as

$$\mu_B = q_{b,B}\mu_n - q_{e,B}\mu_e \ , \tag{64}$$

where $q_{b,B}$ is baryon number of particles and $q_{e,B}$ denotes electric charge of particles, giving set of equilibrium equations

$$\begin{aligned}
\mu_\Lambda &= \mu_n \ , \\
\mu_{\Sigma^-} &= \mu_n + \mu_e \ , \\
\mu_p &= \mu_n - \mu_e \ , \\
\mu_\mu &= \mu_e \ .
\end{aligned} \tag{65}$$

Neutrinos escape from stable neutron star since the density is not sufficient to confine them, thus their energy diminishes and is not involved. The next natural constraint is total baryon density given by Eq. (60).

A lifetime of neutron star compared to high energy collision typical timescale indicates that the main difference between matter in high energy collisions and

β stable nuclear matter in neutron star is a nonconservation of baryon number (due to presence of leptons) and zero electric charge of the system. This can be expressed as charge neutrality condition

$$\rho_p = \rho_e + \rho_\mu + \rho_{\Sigma^-} \ . \tag{66}$$

Thus, self-consistent simultaneous calculation of twelve equations - hyperon matter mesons potentials (52)-(57), set of chemical potential relations (65), total baryon density (60) and charge neutrality (66) - has to be performed to obtain properties of hyperon matter in β equilibrium.

4 The Goal

Nuclear matter is constantly a current topic of research, serving as a starting point for a study of several problems of nuclear physics and astrophysics. An effort to understand the structure and properties of finite nuclei is one of them that has led to developing of non-relativistic Brueckner-Hartree-Fock approach [134]. However, in spite of a relative success, after applying to the calculations of properties of nuclei in a ground state some discrepancies with the experimental results still remained there. These were substantially reduced by developing of a relativistic enhancement of BHF approach, the so-called Dirac-Brueckner-Hartree-Fock (DBHF) method, that enables deeper understanding of the relation between nuclear structure and NN-interaction [135, 136]. Its principle is an usage of Dirac equation for description of one-particle motion in nuclear matter. The Dirac spinor entering calculation of nucleon-nucleon potential becomes density dependent here. Just this additional density dependence is essential for correct reproduction of saturation density and binding energy of nuclear matter. NN-potential obtained is then fitted to the nucleon-nucleon scattering data and deuteron properties. A great effort has been devoted to the successful DBHF description of the symmetric and asymmetric nuclear matter [135, 136, 137].

However, the DBHF approach is very complex and elaborate even in the case of nuclear matter. Fully consistent application to finite nuclei description has not been achieved yet.

This restriction can be partially overcome either by fitting of the free parameters of mean-field theory to the results of calculations of DBHF theory for nuclear matter [130] which provides an effective parametrization of DBHF theory and indirect connection to nucleon-nucleon potential, properties of finite nuclei as well as properties of neutron stars; or via using of the density dependent coupling approach [138].

Many works have dealt with DBHF description of symmetric and asymmetric

nuclear matter (e.g., [139, 140, 141, 137]). Besides nuclei near the stability line description of nuclei with high isospin asymmetry is important as well. Also the matter of final stages of star evolution is neither symmetric nor neutron one. Similarly in high energy ion collisions there are nuclei created with high excess of neutrons. Thus, an inevitable step in description of such systems is an enhancement of isospin degree of freedom. In accordance with this trend also DBHF calculations progress in this direction [137, 142]. Therefore, the first aim of this work is to apply the concept of Ref. [130] also to asymmetric nuclear matter with parameters simultaneously fitted to binding energy per nucleon as well as to isoscalar and isovector meson potentials.

Another aim is to examine an additional enhancement of isovector sector by involving isoscalar-isovector cross interaction into calculations. We will especially concentrate on its influence on nuclear symmetry energy. Dynamical collisions between neutron-rich nuclei shows the main reaction mechanism including fragmentation is highly sensitive to symmetry energy density dependence [143]. It is possible to obtain experimentally its value for nuclear matter at saturation density (nowadays 30 ± 4 MeV [144]) from systematic study of atomic nuclei masses. In this way it is determined only in narrow asymmetry and density window. Thus, only little attention had been paid to it in the past, due to unreliable extrapolation to high densities. Nevertheless, also here the situation has changed last years, with progress in development of ion beams which produce nuclei with higher neutron excess. It is possible to experimentally study density dependence of the symmetry energy through relativistic ion collision where matter at two-three times of the saturation density is produced. This is the reason of intense theoretical attention paid in last years. Thus, another aim of this work is a study of the symmetry energy and influence of vector cross interaction on its density dependence.

Due to developing experimental techniques and facilities it is possible nowadays to reach densities of several times of the saturation density. Similarly also

astrophysical observations are still improving their precision and reliability. It naturally brings a necessity of theoretical extrapolation of nuclear matter calculations to the higher densities. One way is an incorporation of heavier baryon states - hyperons. Neutron star being practically a gigantic atomic nucleus creates an opportunity to connect nuclear physics with astrophysics. Neutron star matter is a nuclear matter in β equilibrated state. Thus, to obtain neutron star matter properties we must calculate properties of matter containing protons, neutrons, hyperons and due to β stability also electrons and muons.

5 Obtaining the Parametrizations

The mean-field parametrizations were obtained by calculation using three different DBHF results for nuclear matter as initial data - results of Li, Brockmann and Machleidt [145], results of Lee, Kuo, Li and Brown [146] and finally calculations of Huber, Weber and Weigel [147]. The differences between them will be discussed in the next subsections.

Original program codes were developed in order to calculate nuclear matter properties as well as properties of hyperon matter in β-equilibrium. Moreover, the MINUIT (Function Minimization and Error Analysis) package available at CERN Program Library [148] was used for the optimization procedure, employing the least squares method which can be formally written as a minimization of a functional:

$$\chi^2 = \sum_i \frac{\left[y_i - y(\vec{a})\right]^2}{\sigma_i^2} \ , \tag{67}$$

where y_i represents DBHF results and $y(\vec{a})$ denotes mean-field calculation with parameters $\vec{a}$, the term σ_i^2 being correspondent statistical weight.

5.1 Fitting Symmetric and Neutron Matter Properties

Based on the realistic and relativistic NN interaction of the Bonn group, in Ref. [145] there were performed DBHF calculations that yield effective NN interactions, and subsequently the single-particle potentials, equations of state, nucleon effective masses, and speed of sound for both symmetric and neutron matter were studied. The Bonn A potential reproduced quantitatively the empirical saturation properties of nuclear matter as well as nucleon effective mass.

As it is easily seen from the equations for meson potentials and for the energy per nucleon, the squares of coupling constants appear exclusively in fraction with meson masses and thus one can fix the meson masses to the experimental values without any physical restriction of the MFT. The meson masses considered in

Table 6: Parameter sets resulting from the fit of Machleidt *et al.* [145] DBHF results (for nucleon-meson coupling constants).

	Ma92A	Ma92B
g_σ^2	106.85	112.27
g_ω^2	180.61	204.36
g_ρ^2	18.445	9.4932
b_σ	-0.0025823	-0.002982
c_σ	0.011529	0.013345
c_ω	0.015849	0.020449
Λ_V	0.25857	—
χ^2/N	2.76	9.95

this work are listed together with other properties and particles in Tab. 4.

The fit was performed using nucleons, σ, ω, and ρ mesons as degrees of freedom, then scalar isoscalar cubic and quartic self-interactions, vector isoscalar quartic self-interactions, and vector-isovector cross interaction, fitting energies per nucleon for symmetric and neutron matter and symmetric isoscalar potentials. The corresponding parameter sets obtained with (Ma92A) and without VCI (Ma92B) are listed in Tab. 6.

The energy density of the system per nucleon dependent on baryon density is shown in Fig. 5. The DBHF results are represented by symbols (squares for neutron matter and circles for the symmetric nuclear matter), and lines denote results of the fit where the solid lines correspond to parametrization Ma92A with VCI included, while the dotted lines are results where VCI have not been taken into account. The saturation mechanism as an important feature of the relativistic field theoretical models is clearly seen, making nuclear matter stable bounded at approximately -16 MeV per nucleon and at the density 0.17 fm^{-3}. Neutron matter is unbound, feeling only slight saturation "valley" (and only gravitation enables the neutron matter in neutron stars to be in bound state). Both of these parametrizations reproduce the DBHF results satisfactorily in whole fitting range of densities relevant for common nuclei which can be said both for the energy

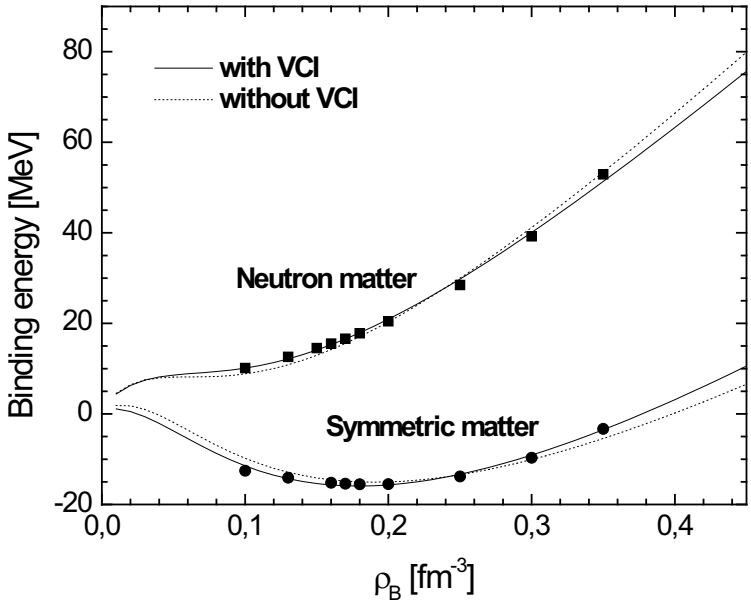

Figure 5: Density dependence of binding energy per baryon for both neutron and symmetric matter as resulted from the fit (represented by lines) to DBHF calculations of Machleidt *et al.* [145] (symbols). Solid and dotted lines correspond to parametrizations Ma92A and Ma92B, respectively (see Tab. 6).

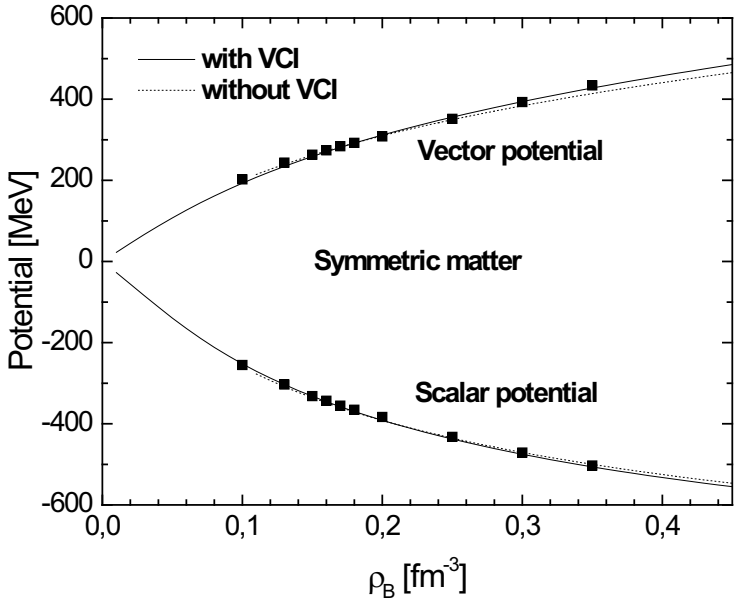

Figure 6: Density dependence of scalar and vector meson potentials in symmetric matter, notation is the same as in the previous Fig. 5.

per nucleon and also for the isoscalar σ and ω meson potentials. However, the inclusion of an additional degree of freedom - VCI - slightly improves reproduction of starting data, especially at the boundary fitted density regions which applies mainly to the energy density for symmetric matter where there is some divergence (that - as it will be shown through the next parametrizations - can be corrected by incorporation of additional asymmetries). This is naturally connected with lower χ^2/N value that is roughly 3.6 times lower in Ma92A compared to Ma92B. In Fig. 6 we can see density dependence of isoscalar scalar σ and vector ω potentials, with the same notation as in the previous figure. It demonstrates that in spite of small binding energy per nucleon the isoscalar potentials are of the order of several hundreds MeV, at the saturation density being roughly 300 MeV. Also in this case the reproduction of the original DBHF data is fair, again with slightly better vector potential values in Ma92A, with scalar potential almost untouched due to pure vector nature of VCI. For this reason much more distinct difference between these two parametrization sets is visible from Fig. 7 where in absence

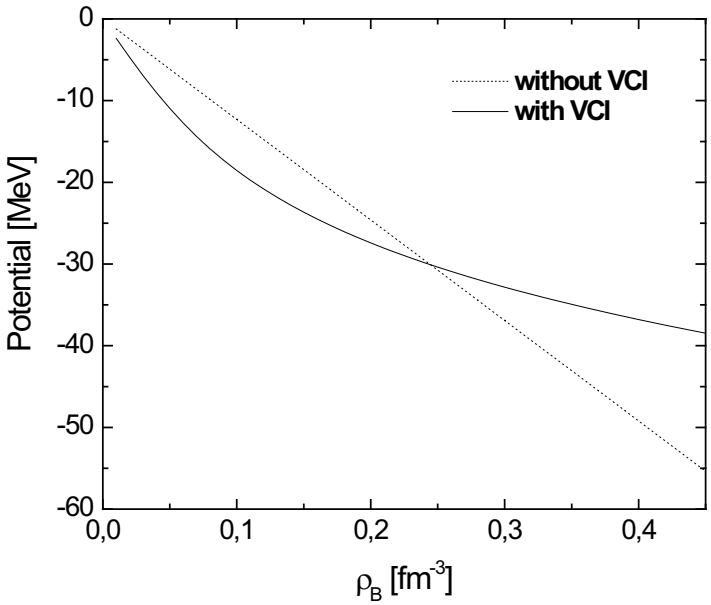

Figure 7: Density dependence of ρ meson potential in pure neutron matter, notation the same as in previous figures.

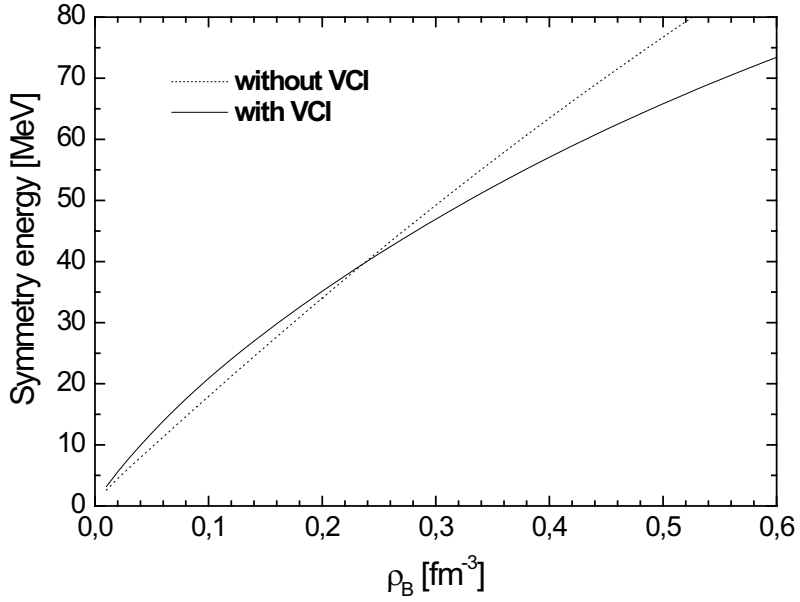

Figure 8: Density dependence of symmetry energy calculated from parametrizations Ma92A (with vector cross interactions) and Ma92B (without VCI).

of VCI the growth of the ρ potential is linear (dotted line). If VCI are switched on the ρ potential slope is decreasing with baryon density. The effect is stronger than in ω meson case also due to lower value of isovector potential and binding of ω potential to DBHF data through the fit procedure. An impact on curvature of the symmetry energy which is plotted in Fig. 8, is very interesting. The cross interactions significantly affect density dependence of the symmetry energy - they increase the rise of symmetry energy below 0.24 fm^{-3} and decrease it above this density. Symmetry energy at the saturation density is 33.3 MeV which is in accordance with the experimental value of about 30 MeV. The uncompressibility of symmetric matter at the saturation density is 347 MeV.

5.2 Incorporating Additional Asymmetries

Symmetric and neutron matter are extreme cases of isospin asymmetry, however, almost no objects in the universe are of such a pure nature. Thus, intermediate asymmetries would improve description of nuclear matter properties. The Ref.

Table 7: Parameter sets with (Le98A) and without cross interaction (Le98B) resulting from the fit of Lee *et al.* [146] DBHF results.

	Le98A	Le98B
g_σ^2	103.91	102.11
g_ω^2	147.84	146.73
g_ρ^2	17.432	9.6697
b_σ	0.00097186	0.00083559
c_σ	0.0012694	0.0012411
c_ω	0.0054204	0.0051878
Λ_V	0.18790	—
χ^2/N	1.69	2.62

[146] deals with asymmetric matter also using the DBHF approach with Bonn A one-boson-exchange NN interaction. Not only saturation properties but, in addition, even the empirical value of the symmetry energy at the saturation density were reproduced satisfactorily. Authors have calculated also isoscalar meson potentials for symmetric matter.

Results of the fit with the same degrees of freedom as were in the previous case performed for binding energy per nucleon for several asymmetries, ranging from symmetric matter to Z/A=0.2 as well as for symmetric matter scalar and vector potential, are listed in Tab. 7. Parameter set obtained using model without vector meson cross interactions is also added. All of the relevant physical quantities for all of the asymmetries are reproduced closely, which can be seen in Fig. 9 where similarly as in Fig. 5 energy density per baryon in dependence on baryon density for parametrization with (Le98A, solid lines) and without VCI (Le98B, dotted lines) is plotted. Especially pure neutron matter and symmetric matter for lower densities are nicely reproduced due to cross interaction influence.

Fig. 10 shows density dependence of calculated isoscalar potentials compared to DBHF results where MFT calculations follow DBHF results very closely too. Isovector vector potential for three different asymmetries is drawn in Fig. 11. VCI inclusion (solid line) indicates similar behavior compared to their absence

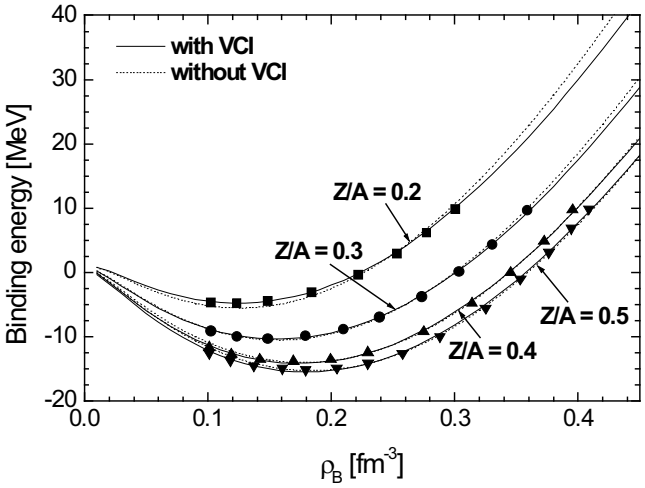

Figure 9: Density dependence of binding energy per baryon as resulted from the fit (represented by lines) to DBHF calculations of Lee *et al.* [146] (symbols). Solid and dotted lines correspond to parametrizations Le98A and Le98B, respectively (see Tab. 7). The fits were performed for several asymmetries ranging from symmetric matter (Z/A=0.5) to highly isospin asymmetric matter with proton population of 20%.

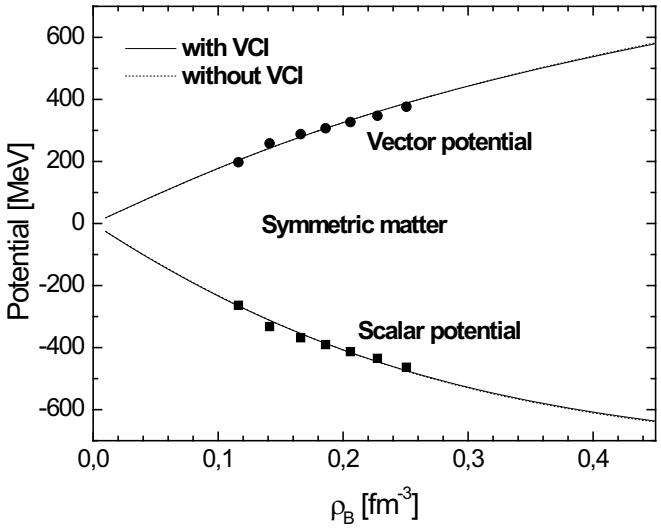

Figure 10: Density dependence of scalar and vector meson potentials in the symmetric matter, notation is the same as in the previous Fig. 9.

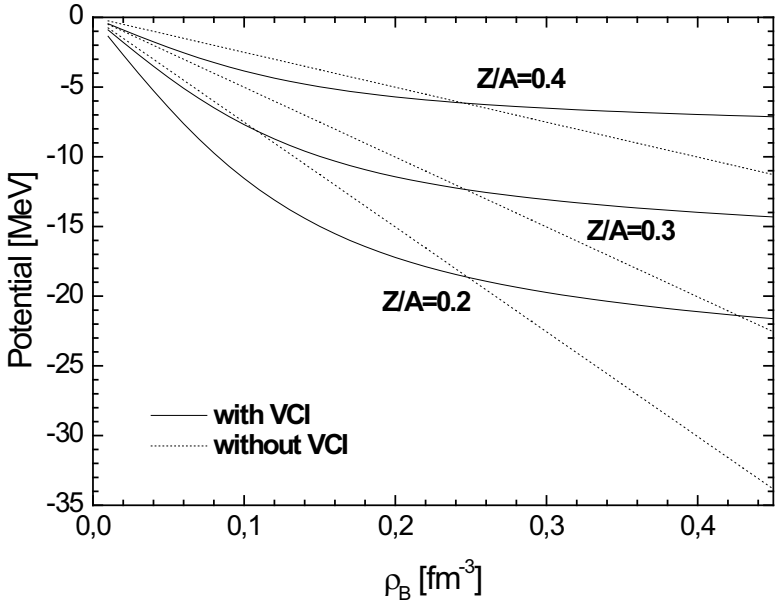

Figure 11: Density dependence of isovector vector ρ meson potential for three different asymmetries as resulted from parametrizations Le98A (with VCI) and Le98B (without VCI).

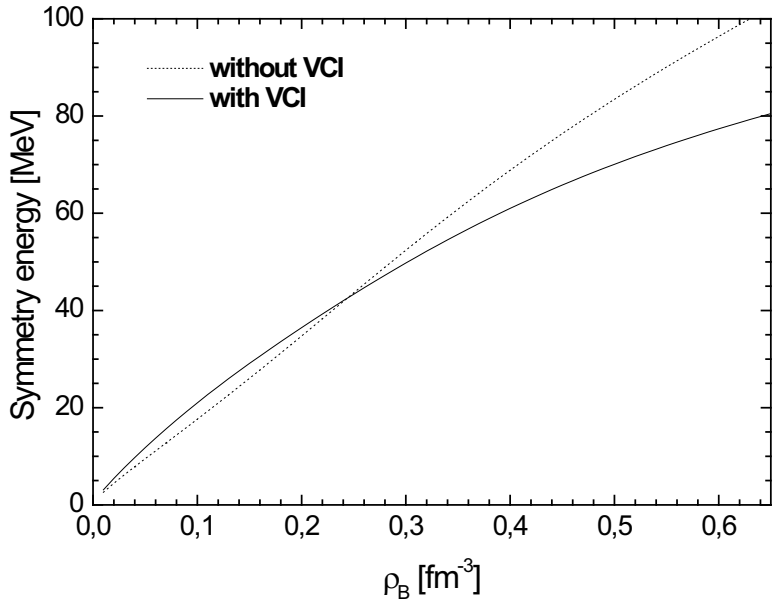

Figure 12: Density dependence of symmetry energy calculated for parametrizations Le98A (solid lines) and Le98B (dotted lines).

(dotted lines) as in the previous parametrizations, for all of the asymmetries, towards higher densities the attenuation of the potential rise is even stronger, thus leading almost to some saturation plateau.

Calculations of VCI influence on symmetry energy behavior indicate that also for this case there is increasing growth of symmetry energy below approximately 0.25 fm^{-3} and slower one in higher density region, as it is drawn in Fig. 12. This fact will be commented more closely in the last data set.

5.3 Isovector Sector Enhancement

Description of nuclear matter with high isospin asymmetry requires incorporation of the isovector sector into calculations. In the previous sets this sector was represented by isovector vector ρ meson field. It could be expected that an enhancement of this sector should lead to a better description of properties of nuclear matter as well as finite nuclei. Thus, we included into calculation also additional degree of freedom - isovector scalar δ meson field. Mass and quantum numbers of this meson are listed in Tab. 4.

In Ref. [147], the energy per nucleon for several asymmetries by using DBHF approach, potential Bonn B, has been calculated. Together with proton and neutron scalar and vector potentials it enables to fit the mean-field parameter for

Table 8: Parameter sets resulting from the fit of Huber *et al.* DBHF results [147].

	Hu95A	Hu95B	Hu95C	Hu95D
g_σ^2	90.532	86.432	91.110	87.591
g_ω^2	108.95	106.89	109.26	107.61
g_ρ^2	36.681	28.795	20.804	15.335
g_{δ^2}	28.739	25.170	—	—
b_σ	0.0043852	0.0033779	0.0044388	0.0035745
c_σ	-0.0052045	-0.0037762	-0.0052076	-0.0039753
c_ω	-0.0001421	-0.001050	-0.00003851	-0.0007753
Λ_V	0.10647	—	0.34805	—
χ^2/N	2.05	3.80	5.85	6.89

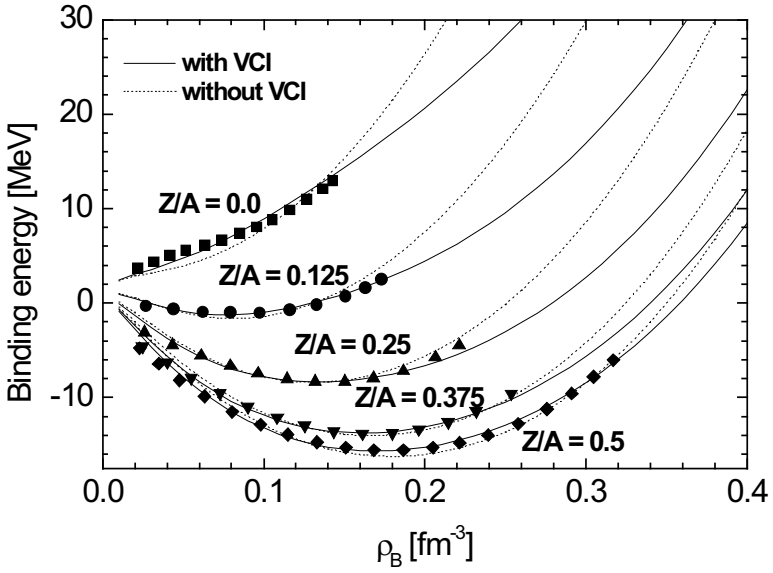

Figure 13: Density dependence of binding energy per baryon as resulted from the fit (represented by lines) to DBHF calculations of Huber *et al.* [147] (symbols). Solid and dotted lines correspond to parametrizations Hu95A and Hu95B, respectively (see Tab. 8). The fits were performed for five different asymmetries ranging from symmetric matter (Z/A=0.5) to pure neutron matter (Z/A=0.0).

coupling of δ meson to nucleons. In this work, furthermore, there has been tested also momentum dependence of self-energies, however, due to momentum independence of mean-field theory coupling constants, the momentum independent results were chosen to fit.

Parametrizations obtained from these fits are listed in Tab. 8. Unlike in the previous cases we decided to test quaternion of sets: the first Hu95A is full parametrization which contains both VCI and δ meson, the second one Hu95B is without VCI but includes δ meson. The third parametrization on the contrary excludes δ meson while it simultaneously incorporates VCI, and finally the quaternion closes with parameter set Hu95D that takes into account neither VCI nor δ meson degrees of freedom.

Starting DBHF data for energy density per baryon together with calculation results are with the same notation as in the previous subsections plotted in

Fig. 13. Five different asymmetries taken into account range from pure neutron matter to symmetric matter. All of the asymmetries are reproduced well within whole fitting density region, with relatively small difference of VCI inclusion or exclusion. However, at higher density these differences cause significant change of energy density behavior, especially for high isospin asymmetry. This is evoked by softening of nuclear matter equation of state that is a direct VCI effect - nuclear matter is less resistant against compression (incompressibility is reduced from 297 MeV to 232 MeV, and this effect is only slightly influenced by δ meson - in that case reduction is from 284 MeV to 232 MeV). Also in the previous two DBHF sets this effect should appear. Its intensity is smaller in Le98A and B parametrization set - reduction is from 317 MeV to 302 MeV. Ma92A and B set gives very small and opposite difference from 342 MeV to 347 MeV. This is due to not fitting intermediate asymmetries and thus relatively less accurate reproduction of energy density for symmetric matter which was improved by VCI inclusion. Thus, this effect is discussed here where the physically natural consequence of VCI-induced softening of nuclear matter equation of state is mostly distinct.

Fig. 14 shows us the second part of fitted quantities - symmetric isoscalar potentials. There is nothing surprising in this figure, fit reproduces DBHF results very well. Above-mentioned proton and neutron scalar and vector potentials which enable fitting also δ meson coupling to nucleons are drawn in Fig. 15, for proton fraction equal to 12.5%. We can see that neutron feels stronger both scalar and vector meson field. All of DBHF potentials are closely followed by calculated fit results. Difference caused by VCI is evident mostly in neutron vector potential.

Interesting evaluation of δ and VCI influence on nuclear symmetry energy is possible from Fig. 16. Influence of the cross interactions is relatively independent on presence of δ meson, while δ meson effect is smaller and opposite in VCI presence. It contributes positively to symmetry energy if VCI are present and negatively in their absence. However, at higher densities (see inset Fig. 16) it appears that while positive contribution of δ meson rises with density, negative

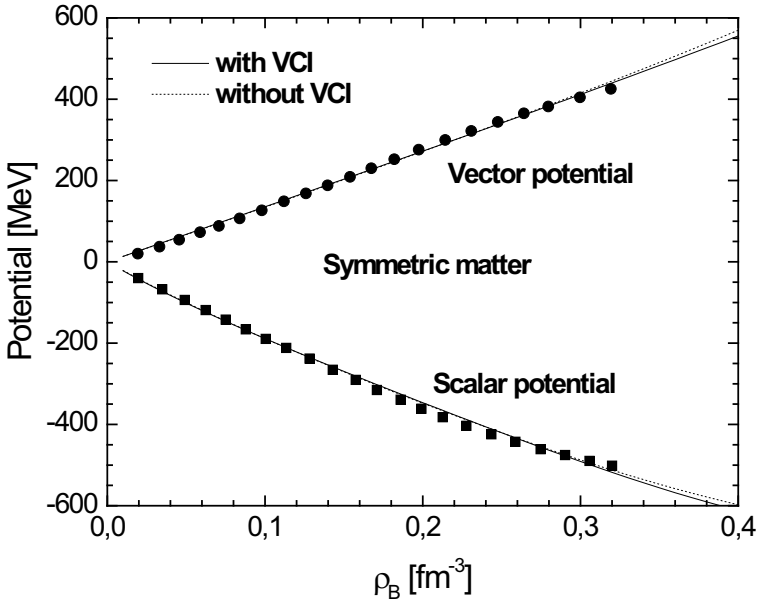

Figure 14: Density dependence of scalar and vector meson potentials in symmetric matter, notation is the same as in the previous Fig. 13.

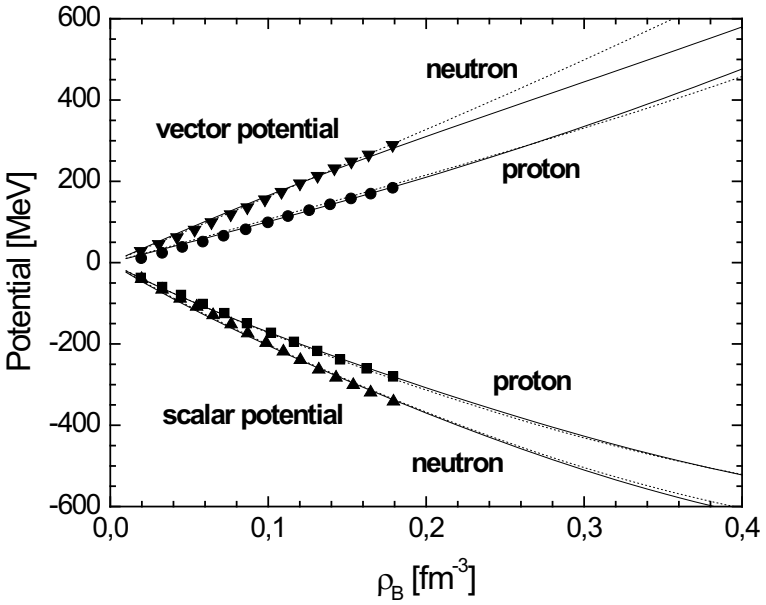

Figure 15: Proton and neutron scalar and vector potentials for asymmetry Z/A=0.125, notation is the same as in previous figures.

contribution (in VCI presence) turns into positive at higher densities, though both still remaining close to each other. Thus, in this case VCI eliminates δ meson contribution to the symmetry energy, indicating that change in its isovector Lorentz structure caused by cross interaction of ρ meson is sufficient, and there is only a weak need for isovector scalar meson introduction. Nevertheless, the general trend of the symmetry energy density dependence shape supports results of the previous two parametrization sets.

An interesting progress has been achieved during recent years in experimental knowledge of the symmetry energy density dependence and due to new facilities it may be expected to continue. Density dependence of the symmetry energy at low energies is closely connected to, e.g., thickness of finite nuclei neutron skin [149] (since its slope is related with a pressure that pushes neutrons out against the surface tension of the nucleus). It is also well known that the π^+/π^- ratio in heavy-ion collisions depends strongly on the isospin asymmetry of the reaction system, and is uniquely determined by the high density behavior of the symmetry

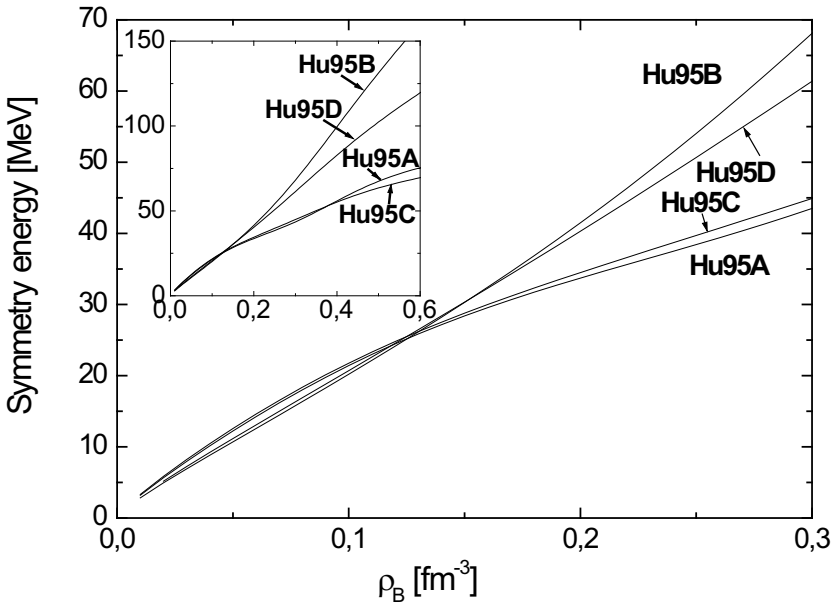

Figure 16: Density dependence of symmetry energy calculated from four different parametrizations Hu95A - D. Higher density region is shown in the inset figure.

energy [150]. Also neutron and proton collective flow measurements seem to represent a very nice exploration of asymmetry properties of matter [151]. Thus, study of neutron distributions in n-rich nuclei (stable and unstable), experiments with heavy ion collisions at intermediate energies (dissipative mechanisms, fast nucleon emission, collective flows) and high-energy radioactive beams are very efficient tools for probing the density behavior of the symmetry energy. Other possibilities are, e.g., assessment of drip-line stabilities [152].

Thus, also the theory tries to describe better the symmetry energy behavior. The results can be roughly classified into two groups, one where symmetry energy rises (*Asy-stiff*), and one in which it falls with increasing density (*Asy-soft*) [153]. A general problem of conventional mean-field models is overestimating of the symmetry energy value at higher densities in comparison with realistic non-relativistic potentials and DBHF calculations [154]. An implementation of isovector degrees of freedom has improved the situation, as it follows also from the results of this work. However, also different approaches successfully deal with this problem, like models incorporating a point coupling [155] or density dependent Hartree-Fock [138].

The influence of δ meson on symmetry energy density dependence within relativistic mean-field theory has been recently examined also in Ref. [156]. Authors obtained the same results for higher densities - isovector scalar meson makes the symmetry energy more repulsive. This is a consequence of a different Lorentz structure - similarly as in the isoscalar sector there is a natural cancellation between isovector scalar and vector meson fields. This cancellation is less effective at higher densities, with the repulsive ρ meson gaining more importance. With this pure relativistic mechanism the inclusion of δ field makes the symmetry energy more repulsive at higher densities. Similar results are given also by a nonlinear Hartree model [157, 158].

6 Hyperon Matter in β Equilibrium

Incorporation of hyperons into the model is straightforward - one only needs appropriate additional terms in lagrangian density, as it was done in Eq. (39). However, there also appear additional couplings which need to be determined or at least constrained satisfactorily that means in concordance with available experimental data.

6.1 Finding Hyperon Couplings

As it was mentioned in the theoretical section of this work, due to poor experimental data in the field of hypernuclei and hyperon-nucleon and hyperon-hyperon interaction we have constrained couplings of hyperons to vector and isovector mesons by quark model (41).

Contemporary experimental knowledge of hypernuclei and double-hypernuclei enables us to determine rough value of potential depth felt by hyperons in nucleonic matter (42) and hyperonic matter (43).

Table 9: Hyperon-scalar meson couplings for Ma92A and B parametrizations (see Tab. 6) and for Le98A and B parametrizations (see Tab. 7) resulting from the fit to hypernuclear potentials (42,43). Hyperon-vector (isovector) meson couplings ensue directly from (41).

	Ma92A	Ma92B	Le98A	Le98B
$g_{\sigma\Lambda(\Sigma)}/g_{\sigma N}$	0.6072	0.6041	0.6078	0.6062
$g_{\sigma^*\Lambda(\Sigma)}/g_{\sigma N}$	0.7851	0.7852	0.7533	0.7541

Table 10: Hyperon-scalar meson couplings for Hu95A - D parametrizations (see Tab. 8) resulting from fit to hypernuclear potentials (42,43).

	Hu95A	Hu95B	Hu95C	Hu95D
$g_{\sigma\Lambda(\Sigma)}/g_{\sigma N}$	0.6120	0.6065	0.6123	0.6076
$g_{\sigma^*\Lambda(\Sigma)}/g_{\sigma N}$	0.7601	0.7635	0.7603	0.7624

To meet this constraints, we have performed fit of the relevant couplings for each of parametrizations listed in Tab. 6, Tab. 7 and Tab. 8. Results of these fits are listed in Tab. 9 and Tab. 10. For all of the parametrizations we can see very close values of $g_{\sigma\Lambda(\Sigma)}/g_{\sigma N}$ equal roughly 0.61, arisen from similar balance of isoscalar potentials near the saturation density. Inclusion of VCI has only minor effect on this value that also applies to the fraction of couplings $g_{\sigma^*\Lambda(\Sigma)}/g_{\sigma N}$. However, in this case there is some difference between particular parametrization sets, the values are approximately 0.79, 0.75, and 0.76 for Ma92A and B, Le98A and B, and Hu95A-D parameter sets, respectively. This is also a consequence of lower values of strange meson potentials in hyperonic matter compared to isoscalar potentials and thus it is needed a more distinct shift of coupling values to maintain the constrain (43).

6.2 Hyperon Matter Properties

Hyperonic matter in β equilibrium is characterized chiefly by its composition, i.e., by density dependence of relative abundance of its particular components, and by meson potentials. Also some other quantities, such as an electron chemical potential, can be interesting and important. They will be analyzed in the next subsections.

6.2.1 Composition of Hyperon Matter

Density dependence of relative abundance of particles of which the hyperonic matter consists, is the result of self-consistent simultaneous calculation of all of the meson potential equations and equilibrium equations. We have considered β-stable hyperonic matter consisting of protons, neutrons, Σ^-, Λ^0 hyperons, electrons and muons. We didn't take into account other types of hyperons, because the heaviest $\Delta^{\pm}{}_{0}{}^{,++}$ seem to be suppressed [159, 110], and also other baryons (Σ^{0},Ξ^{0}) due to their electric charge or higher rest mass may appear only at very high densities or may not appear at all [160]. Since our parametrization sets

result from fit up to densities around 0.33 fm^{-3}, reliability of the extrapolation to such a high density is less approved. Moreover, it seems that at least some important matter properties are more affected by total hyperonization than by hyperon subtypes themselves which is indicated, for example, by very similar influence of hyperons on electron chemical potential with presence or with total exclusion of Σ^- (due to its possible strong repulsion in nuclear medium) which can be compensated by Ξ^- [125]. Therefore, particular abundance of heavier baryon species is not very important [126].

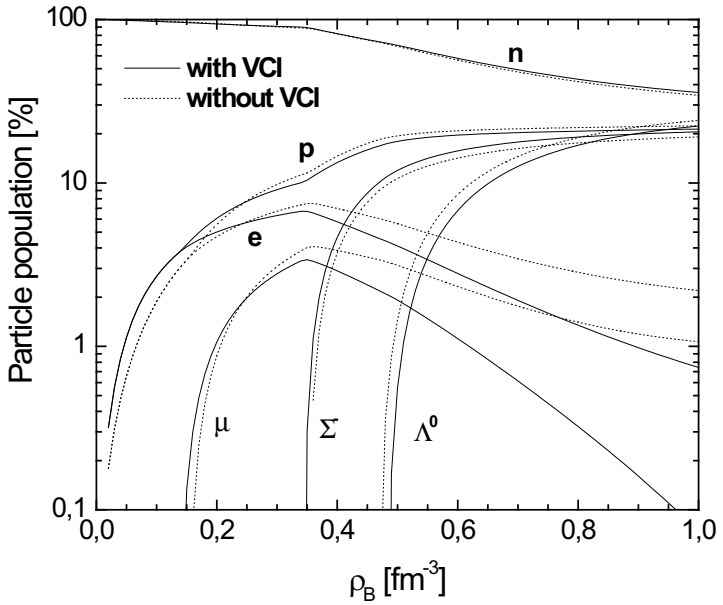

Figure 17: Particle populations in β stable hyperonic matter calculated for parametrizations Ma92A (solid lines, with VCI) and Ma92B (dotted lines, without VCI), listed in Tab. 6 and Tab. 9. Protons, neutrons, Λ^0, Σ^- hyperons, electrons and muons were used in calculations.

In Fig. 17 the results for parametrizations Ma92A and B are shown. Starting from almost pure neutron matter with increasing total baryon density the nuclear matter is enriched by protons and consequently due to charge neutrality also by electrons. Subsequently, the electron chemical potential is rising, and when it reaches value of the rest mass of muon, it becomes possible to turn electron into muon. This happens already closely below the saturation density at $\rho_B = 0.14$

fm^{-3}, and causes also a slight growth of the proton fraction increase. With further rise of density it turns up energetically favorable to turn nucleons with high kinetic energy into heavier baryon resonances. The first hyperon appearing is Σ^- at density 0.35 fm^{-3}, for instance, through reaction

$$n + e^- \longrightarrow \Sigma^- + \nu_e \ . \tag{68}$$

In spite of that Σ^- is not the lightest hyperon, due to its negative electric charge and zero isospin of the lightest Λ^0, it appears before Λ^0 - the electron chemical potential together with ρ meson field affecting Σ^- is higher than Σ^- and Λ^0 effective mass difference. Thus, Λ^0 occurs at densities just above 0.49 fm^{-3}. However, we have to note that quantitative value of threshold densities depends strongly on poorly known nucleon-hyperon coupling constants and their better knowledge will improve correspondence of the theory with reality. In any case onset of hyperons has distinct influence on nucleon and lepton populations. Negatively charged Σ^- heightens proton fraction following by fall of number of both leptons in order to hold charge neutrality of the matter. The lepton population reduction is consequence of local non-conservation of lepton number (neutrinos from Eq. (68) escape from matter). These general characteristics of density dependence of β stable hyperon matter are qualitatively in accordance with other works (e.g., [125, 126, 160, 161, 162]), they differ only quantitatively.

For examination of vector cross interactions, results for parametrization without them (Ma92B) are drawn in the same plot by dotted lines. Since VCI are softening equation of state of nuclear matter, they generally enforce neutron population to the prejudice of protons, with slight shift of muons onset to lower densities and that of Σ^-, Λ^0 to higher densities - without VCI muons appear at 0.16 fm^{-3}, Σ^- at 0.36 fm^{-3} and Λ^0 at 0.47 fm^{-3}.

Another noteworthy matter of fact is that proton fraction also affects the thermal evolution of a star to considerable extent. If its value in the core of star is higher than some critical threshold x_{Urca}, it is possible to turn up direct Urca

process [163]:

$$n \longrightarrow p + e^- + \bar{\nu}_e \ ,$$
$$p + e^- \longrightarrow n + \nu_e \ . \tag{69}$$

This process strongly enhances neutrino emission from protoneutron star and thus its cooling rate. The critical proton fraction ranges between 11–15% [163]. In this case the threshold of 11% is exceeded at density 0.36 fm^{-3} and proton fraction converges to 21% at high densities. Without VCI this values are changed only slightly - the threshold is surpassed at 0.34 fm^{-3} and proton fraction converges to 22% at high densities. Thus, due to threshold surpassing roughly at double of saturation density, there is high probability that direct Urca process occurs in protoneutron star core significantly affecting its cooling rate. This is in accordance also with other works [125, 126, 160, 161, 162].

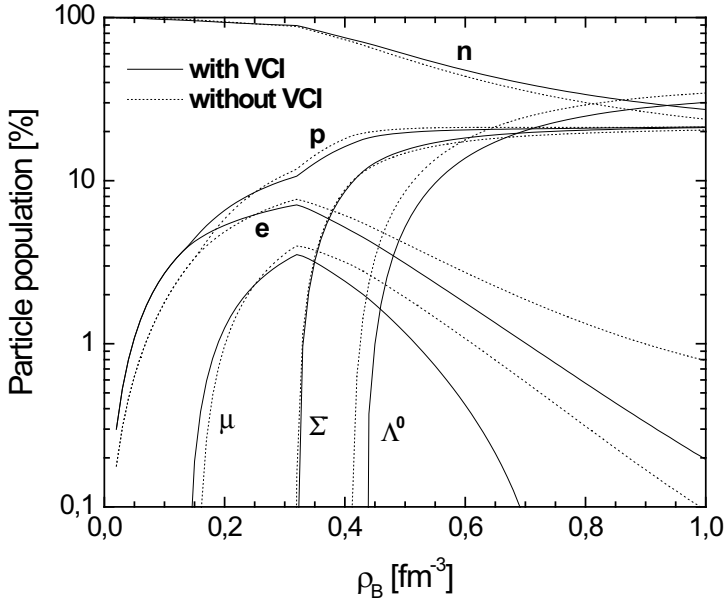

Figure 18: Particle populations in β stable hyperonic matter calculated for parametrizations Le98A (solid lines, with VCI) and Le98B (dotted lines, without VCI), listed in Tab. 7 and Tab. 9.

General features of hyperon matter mentioned above are supported also by results for parametrization sets Le98A and Le98B, drawn in Fig. 18. Here the muons appear at 0.14 fm^{-3} (0.16 fm^{-3}), Σ^- at 0.32 fm^{-3} (0.32 fm^{-3}) and Λ^0 at 0.44 fm^{-3} (0.41 fm^{-3}), values in the brackets being for non-VCI case. The main difference in comparison with previous parameter sets is lower hyperon thresholds and generally richer hyperonization of matter. While in Ma92A and B set the total hyperonization of matter at density $\rho_B = 0.6$ fm^{-3} is 22.5% (22.7%), in Le98A and B results it is 32.0% (35.2%). This is a natural consequence of harder EOS in the second parametrization set. Proton fraction behavior is similar to previous parametrizations - 11 % level for Urca process is surpassed at density 0.33 fm^{-3} (0.31 fm^{-3} without VCI) and converges to 21 % at high densities (for both parametrizations). Thus, also here one can observe possible Urca process starting up at double of saturation density with slight effect of VCI.

Next parametrizations Hu95A-D give outcome plotted in Fig. 19 and Fig. 20.

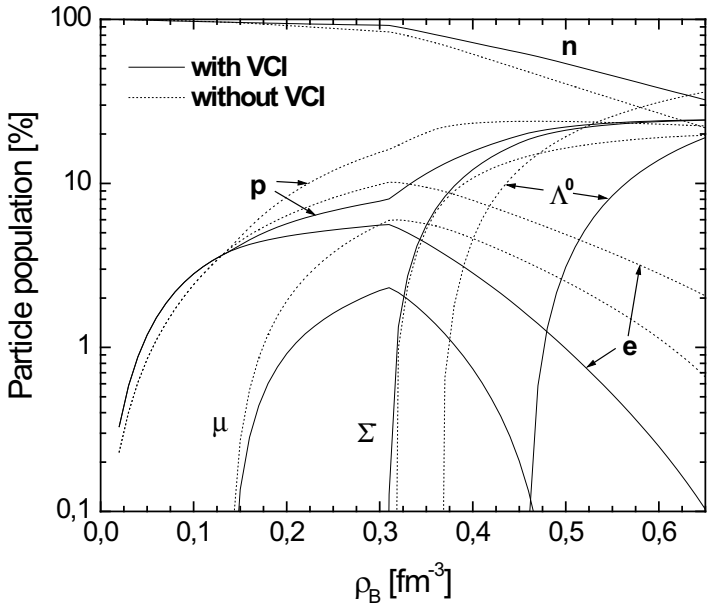

Figure 19: Particle populations in β stable hyperonic matter calculated for parametrizations Hu95A (solid lines, involved both VCI and δ meson), Hu95B (dotted lines, without VCI and with δ meson), listed in Tab. 8 and Tab. 10.

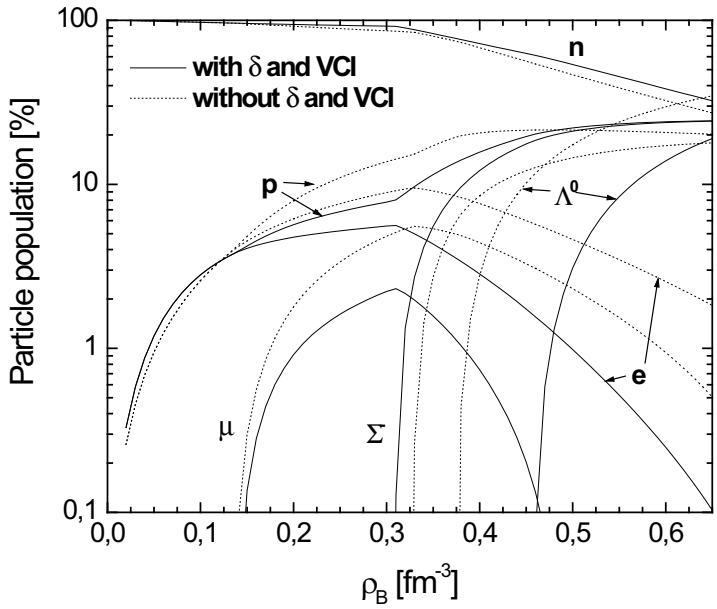

Figure 20: Particle populations in β stable hyperonic matter calculated for parametrizations Hu95A (solid lines, with VCI and δ meson), and Hu95D (dotted lines, neither VCI nor δ meson were involved), listed in Tab. 8 and Tab. 10.

Solid line in both figures denotes particle population density dependence with inclusion of both δ meson and VCI (Hu95A). The influence of VCI absence with simultaneous δ meson inclusion is seen from dotted lines in Fig. 19 (Hu95B), while analogical situation in δ meson absence we can see from dotted lines in Fig. 20 (Hu95D). The VCI effect is more distinct than in previous two parameter sets. First, in a density range roughly from one to two times of the saturation density there is a strong shortage of protons when VCI are present, independently on δ meson. This has strong influence on Urca process start up - without VCI the threshold density is surpassed at 0.35 fm^{-3} with VCI inclusion, but only 0.24 fm^{-3} if they are excluded. Nevertheless, the high density behavior is similar, saturating at fraction of 24% in both cases. The medium density range proton fraction behavior is thus strongly VCI-dependent.

Second important point is distinct shift of Λ^0 threshold to higher densities from 0.37 fm^{-3} to 0.46 fm^{-3} with δ meson or from 0.38 fm^{-3} to 0.44 fm^{-3} without it.

Consequently, the third effect of VCI is more rapid deleptonization of matter - muons are completely extinct already at density 0.50 fm^{-3} with δ mesons or 0.58 fm^{-3} without them. It is clear that VCI play an important role in the equilibrated matter, and it is indispensable physical degree of freedom, supporting conclusions from the previous section.

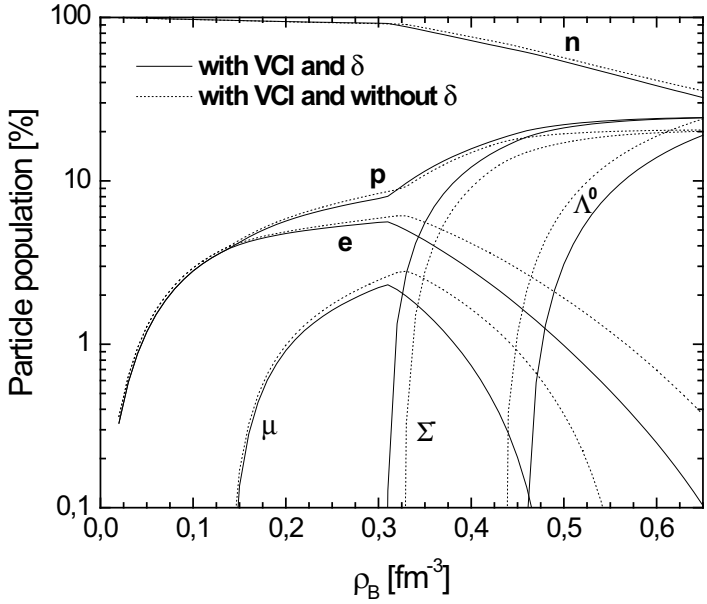

Figure 21: Pure effect of δ meson: particle populations in β stable hyperonic matter calculated for parametrizations Hu95A (solid lines, with VCI and δ meson), and Hu95C (dotted lines, with VCI but without δ meson).

For additional confirmation of this account in Fig. 21 there are drawn particle populations again, both VCI including and explicitly with (solid lines, Hu95A) and without (dotted ones, Hu95C) δ meson. One can conclude that the role of δ meson is of secondary importance, and it doesn't have serious effect on the properties of hyperon matter even at high densities. This is in full agreement with conclusions from Ref. [162]. Finally, as it was already mentioned, VCI soften EOS, in their absence there is higher hyperonization of matter - including (excluding) the isovector-scalar field it is 50.2 % (46.9 %), compared to 37.7 % (38.4 %) at $\rho_B = 0.6$ fm^{-3} if they are switched on.

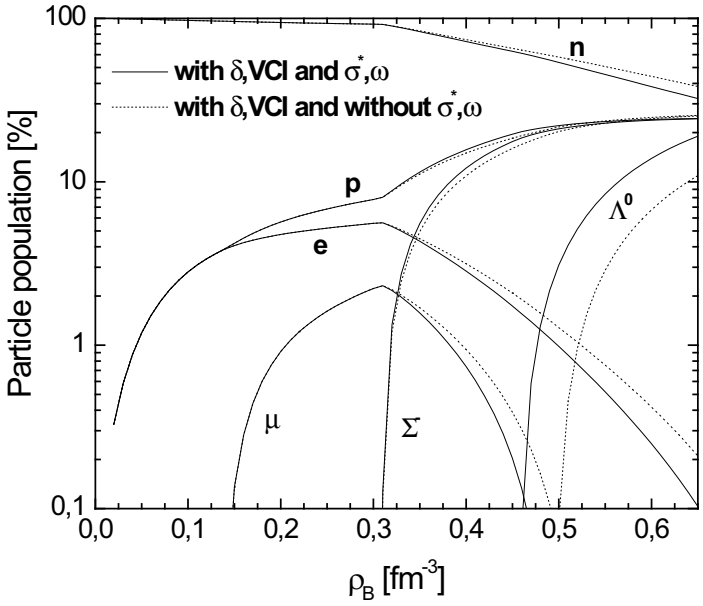

Figure 22: Influence of strange mesons: particle populations in β stable hyperonic matter calculated for parametrizations Hu95A where also (hidden) strange mesons σ^* and ϕ are involved (solid lines), with couplings listed in Tab. 8 and Tab. 10, and for the same parametrizations but without inclusion of these mesons (dotted lines).

In the next Fig. 22 there is examined role of hyperon-hyperon interaction mediated by strange σ^* and ϕ mesons. As they did not couple to nucleons, their effect started up above Σ^- threshold density (which is not affected), and is contradictory to VCI influence, however, of smaller magnitude, thus making the VCI-induced shift of Λ^0 threshold to higher density not so hard. Another effect of strange mesons is stabilization of matter at very high densities. For Le98A and B negative nucleon effective masses appear above 1.89 fm^{-3} (1.76 fm^{-3}) which are changed to positive value if σ^*, ϕ are introduced. Though there doesn't occur also negative electron chemical potential, this is in accordance with results from Ref. [162].

6.2.2 Meson Potentials

Each of the mesons intermediating strong interaction between baryons generates correspondent potential. These potentials we can see in Fig. 23. There are plotted all isoscalar, isovector and strange meson potential as resulted from calculation with parametrization Ma92A (solid lines) and Ma92B (dotted lines). Isoscalar σ and ω potentials are of several times higher magnitude than the others, so for practical purposes they were divided by a factor 10. Their large values clearly indicate that they remain the main contribution to baryon-baryon interaction, thus mostly affecting also balance between scalar and vector meson fields. The secondary vector contribution is isovector ρ potential which is several ten times smaller than its isoscalar counterpart.

Due to self-consistency of the calculations, there is some balance between increasing baryon density and rapid drop of neutron abundance and thus also isospin asymmetry of matter. This balance results in attenuation of isovector ρ

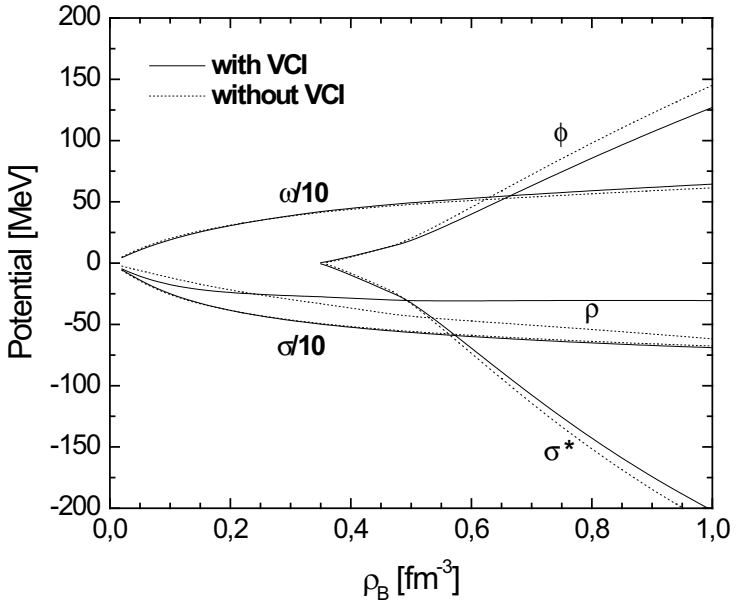

Figure 23: Meson potentials in β stable hyperonic matter, calculated for parametrizations Ma92A and Ma92B (Tab. 6+Tab. 9). Isoscalar scalar σ and vector ω meson potentials are for clarity divided by a factor 10.

potential. When VCI are switched on, they additionally weaken isovector potential which comes to saturation and doesn't exceed 31 MeV at any density. Other meson fields are not so influenceable, although since ω field cross interacts with ρ field, it also exhibits decrease, however, due to much weaker ρ field does not lead to saturation. Strange meson potentials naturally appear just above the first hyperon onset, and have relatively quick rise when reach already about 10% of isoscalar potential values at density 0.6 fm^{-3}. Scalar and vector strange potentials have opposite signs similarly to isoscalar potentials, thus balancing attractive scalar and repulsive vector part of strange interaction. However, scalar σ^* potential softly exceeds its vector counterpart, hence ensuring experimentally observed strong hyperon-hyperon interactions. After an acute onset their rise begins to deescalate, though remaining relatively high. Thus, at higher densities strange meson potentials contribute recognizably to scalar-vector potential balance.

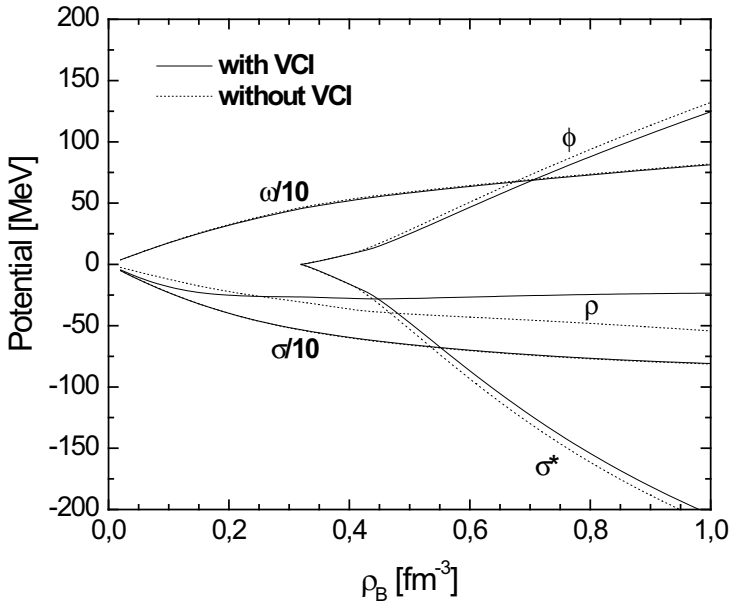

Figure 24: Meson potentials in β stable hyperonic matter, calculated for parametrizations Le98A and Le98B (Tab. 7+Tab. 9). Isoscalar scalar σ and vector ω meson potentials are for clarity divided by a factor 10.

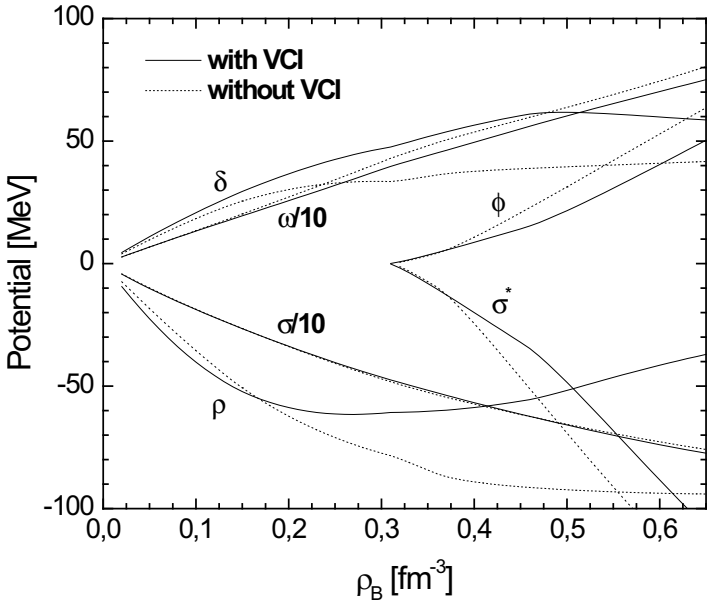

Figure 25: Meson potentials in β stable hyperonic matter, calculated for parametrizations Hu95A and Hu95B (Tab. 8+Tab. 10). Isoscalar scalar σ and vector ω meson potentials are for clarity divided by a factor 10.

In Fig. 24 we can see similar situation for parametrizations Le98A (solid lines) and Le98B (dotted lines). The only differences are slightly higher values of ω potential and lower values of ρ potential, and smaller difference between VCI inclusion and exclusion for strange ϕ potential.

More interesting appears Fig. 25 where meson potentials for parametrizations Hu95A and Hu95B are plotted which means that also isovector scalar potential appears in addition to previous figures. All above described features of potentials remain, except stronger ρ meson field - though in VCI presence it also reaches saturation, the saturation value is about two times higher then in δ meson absence, namely 61 MeV. This is due to opposite effect of isovector scalar and vector mesons which are in this way partially balanced. Weak changes support our previous conclusion and conclusion from Ref. [162] of small δ meson influence. Lower δ meson field in VCI absence is given partially by lower coupling of δ meson to nucleons ($g_\delta^2/g_{\delta\mathrm{VCI}}^2 = 0.88$) needed for proper reproduction of DBHF calcula-

tions as well as by richer proton and Λ^0 and poorer neutron and Σ^- populations, thus resulting in more isospin symmetric matter. As it was already mentioned, VCI soften EOS, in their absence there is higher hyperonization of matter and a natural consequence are stronger strange fields.

6.2.3 Effective baryon masses

A characteristic feature of the mean-field theory is that it describes many-body system as consisting of pseudobaryons with certain effective masses, moving in mean-field potential well. These masses are shifted by value of scalar (isoscalar, isovector as well as strange) meson fields.

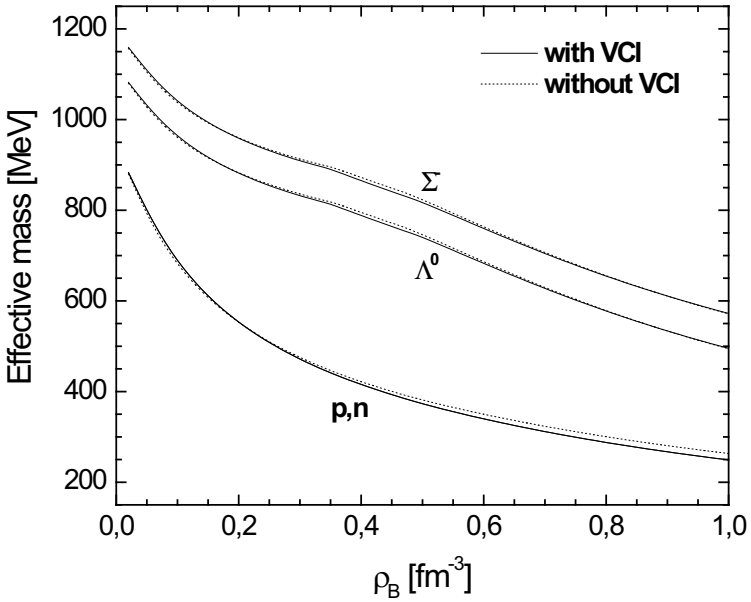

Figure 26: Baryon effective masses in β stable hyperonic matter resulting from parametrizations Ma92A (solid lines) and Ma92B (dotted lines) (Tab. 6+Tab. 9).

Fig. 26 shows density dependence of the effective masses of nucleons, Λ^0 and Σ^- hyperons for parametrizations Ma92A (solid lines) and Ma92B (dotted lines). We can see that they are quickly descending from starting rest masses. The decrease of hyperon effective masses is smaller than that of nucleons which is consequence of weaker strength of hyperon couplings (see Tab. 6). Behavior of

hyperon masses stops being smooth after hyperon onset, due to arising of strange scalar σ^* potential which begins to fortify already softening decrease of hyperon effective masses, hence creating a hump and resulting in diminishing difference between nucleons and hyperons. It can be also seen that VCI have only very mild effect on behavior of effective masses. This can be explained by the fact that the largest contribution to effective mass creates isoscalar scalar potential that is fitted to reproduce the original DBHF calculations.

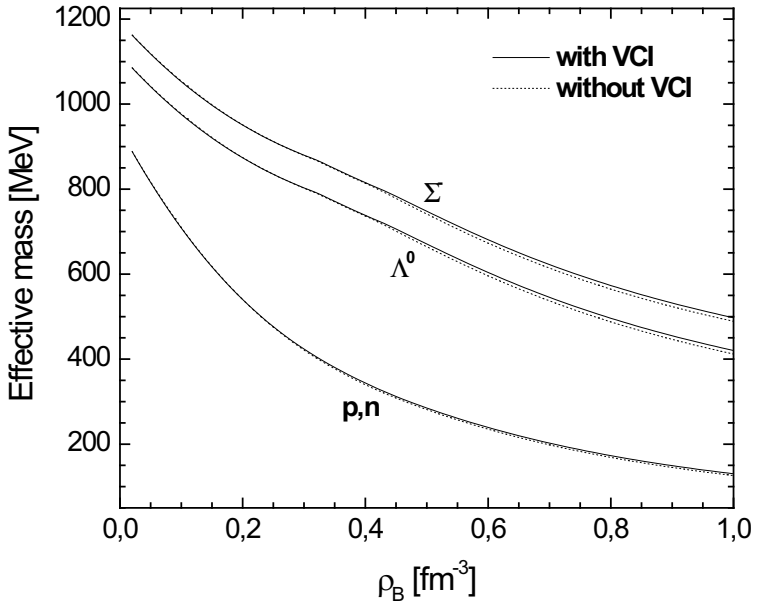

Figure 27: Baryon effective masses in β stable hyperonic matter resulting from parametrizations Le98A (solid lines) and Le98B (dotted lines) (Tab. 7+Tab. 9).

Fig. 27 demonstrates the same situation, but for parametrizations Le98A (solid lines) and Le98B (dotted lines). All qualitative features are identical, however, there is some difference in the effective mass values which are all smaller. Nucleon, Λ^0, and Σ^- effective masses are 25%, 53%, and 56% of rest mass value at 0.6 fm^{-3}, respectively, compared to 37%, 61%, and 64% in sets Ma92A and B (VCI influence is smaller than 1%). This is the consequence of smaller σ DBHF potential of Ma92A and B compared to Le98A and B which naturally emerges also in β stable hyperon matter.

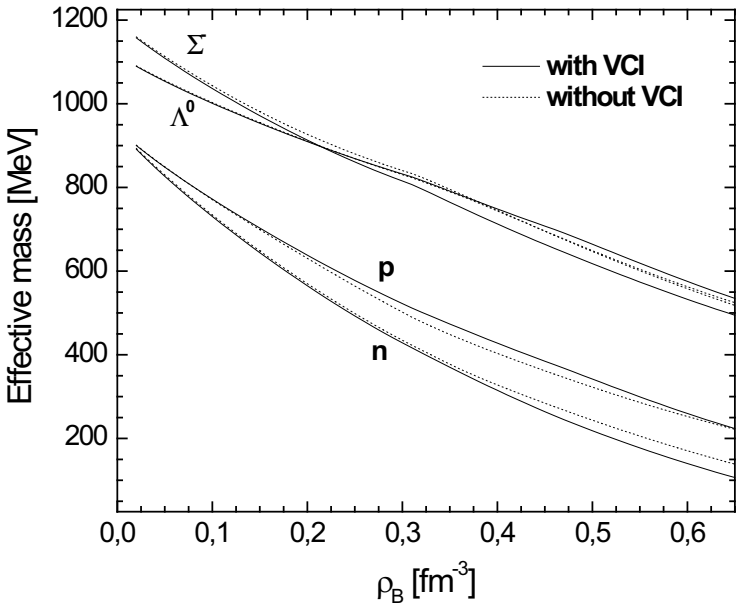

Figure 28: Baryon effective masses in β stable hyperonic matter resulting from parametrizations Hu95A (solid lines) and Hu95B (dotted lines) (Tab. 8+Tab. 10).

Besides a not very strong effect of δ meson on composition of β-stable matter, due to its isospin vector nature it has an impact on effective masses of baryons with non-zero isospin. This one of its most important features is demonstrated in Fig. 28. Unlike in the previous parametrizations, here we can observe clear splitting of proton and neutron effective masses. Additionally, even stronger influence of δ meson is felt also by Σ^- baryon (due to two times larger coupling constant) which is sufficient to cross Λ^0 effective mass at density 0.22 fm^{-3} which is not affected by δ meson ($g_{\Lambda^0\delta} = 0$). However, δ potential saturates around 0.5 fm^{-3}, hence causing a slow decline of neutron-proton and Λ^0-Σ^- mass difference. Here we can see also stronger impact of VCI where weaker δ field leads to crossing of Λ^0-Σ^- at higher density (0.44 fm $^{-3}$), and still remaining close to each other.

6.3 Chemical Potential of Electrons

Hyperon matter equilibrium conditions besides the electric charge neutrality and baryon density sum contains a set of equations for chemical potentials of the

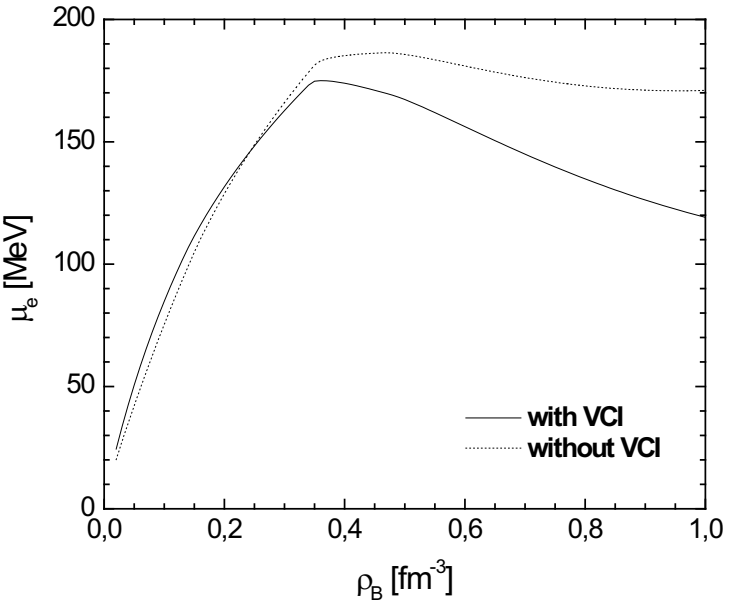

Figure 29: Density dependence of chemical potential of electron calculated for parametrization Ma92A (solid lines, VCI included) and Ma92B (dotted lines, VCI excluded).

particles considered. Electron chemical potential is of a special interest due to its role in kaon condensate appearance, as it will be shown in this section.

Fig. 29 demonstrates main features of electron chemical potential behavior in β stable hyperon matter. Results for parametrization Ma92A (solid line) and Ma92B (dotted line) are plotted. As we can see, with a rising density and abundance of electrons in matter there is also a significant grow of their chemical potential. However, this trend is interrupted when hyperons appear - and this is also one of their important features. Thus, the distinct drop of electron Fermi momentum and concentration in matter after hyperonization is almost immediately followed by a drop of chemical potential which has serious consequences for kaon condensation occurence, as it was first pointed out in Ref. [110]. Vector cross interaction affects both maximum value of the chemical potential and its slope of declining. VCI causes also immediate reduction of chemical potential, while in their absence there is even mild raise after hyperon onset. With VCI the

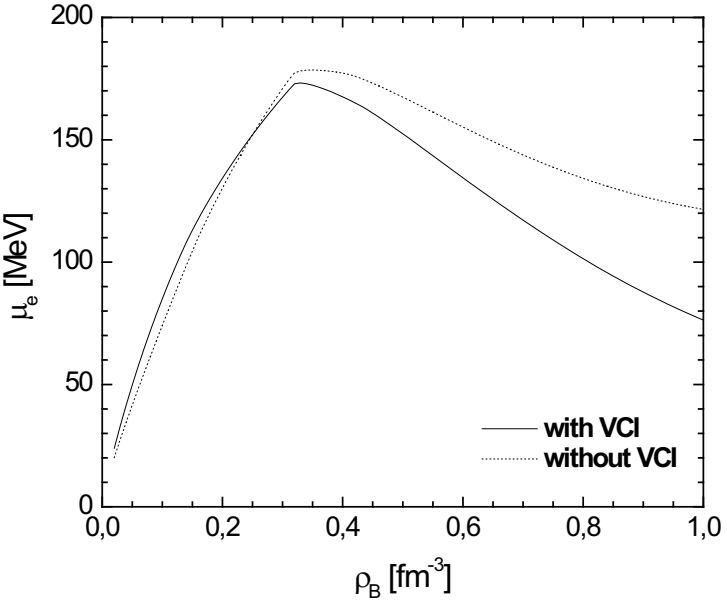

Figure 30: Density dependence of the chemical potential of electron calculated for parametrization Le98A (solid lines, VCI included) and Le98B (dotted lines, VCI excluded).

electron chemical potential saturates at value about 175 MeV and density 0.36 fm^{-3} and the downtrend is roughly continuous till high densities, otherwise saturation point is about 186 MeV at 0.47 fm^{-3}, and the downtrend has tendency to vanish. This difference is directly connected with deleptonization process - the more rapid deleptonization, the more distinct decrease of electron chemical potential.

When we look at parametrizations Le98A and Le98B (solid line and dotted line in Fig. 30, respectively) situation is even more clear. The break of chemical potential is more definite, being 173 MeV at 0.33 fm^{-3} in VCI presence and 178 MeV at 0.35 fm^{-3} in their absence. Also the decline in both cases is more rapid which is a consequence of the stronger deleptonization of matter, and while VCI influence is not strong at the breakpoint density and chemical potential saturation value, they keep their impact on steepness of further decrease.

Even after incorporation of δ meson situation retains qualitatively unchanged,

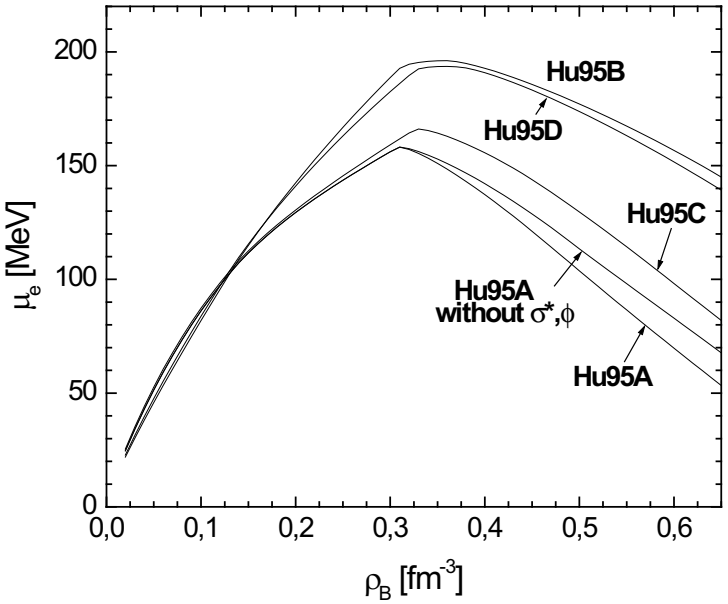

Figure 31: Density dependence of the chemical potential of electron calculated for several degrees of freedom used, represented by parametrization Hu95A - D, listed in Tab. 8 and Tab. 10. Additionally, Hu95A with strange mesons exclusion is also plotted.

as we can see from Fig. 31 where results for all quaternion of parametrization sets are plotted. Without VCI (Hu95B) the electron chemical potential saturates at value about 196 MeV at 0.36 fm^{-3} and δ meson has only a weak effect (about 3 MeV, Hu95D), otherwise saturation value is around 166 MeV at 0.33 fm^{-3} (Hu95C) and even 158 MeV at 0.31 fm^{-3} with δ meson (Hu95A). For comparison also a strange meson influence is demonstrated by result for Hu95A but without them. Due to almost zero strange meson fields at the breakpoint, they have no influence on saturation value, and for higher densities they mildly fortify VCI influence on the electron chemical potential.

As it was already said, the electron chemical potential coheres with kaon condensation onset. This can be more clear from Fig. 32 where two of the previous parametrizations (Hu95A and Hu95B) together with recent effective kaon mass resulting for nuclear matter [164] and neutron matter [165] are plotted. However, its value is continually a current topic of research, and at least for neutron matter

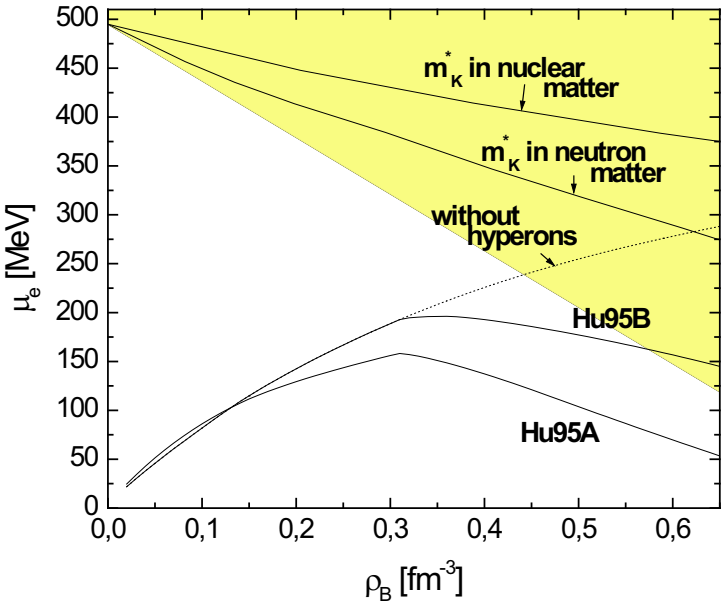

Figure 32: Density dependence of electron chemical potential for two of the parametrization sets from the previous Fig. 31 (Hu95A and Hu95B), together with density dependence of effective kaon mass in nuclear matter (taken from Ref. [164]) and neutron matter (taken from Ref. [165]) are drawn. Filled area denotes possible kaon effective mass in an extreme case of its density dependence, when $m^*_{K^-} = 200$ MeV at treble of the saturation density. For comparison electron chemical potential in the case of hyperon exclusion for parameter set Hu95B is also plotted (dotted lines).

it may be even lower (around 200 MeV at three times of saturation density), as a recent analysis [166] of experimental data [167] suggests. Thus, all possible values of kaon effective mass are plotted as a filled area. If the electron chemical potential reaches effective kaon mass the kaon condensation occurs. Nevertheless, as it can be expected, the electron chemical potential stops rising after hyperonization (otherwise it would continually increase as it shows the dotted line) and starts to decline with increasing density. Vector cross interactions thus lessen probability of kaon condensation at higher densities.

7 Summary

In this thesis the relativistic mean field theory was used to obtain an effective parametrization of the properties of asymmetric nuclear matter calculated by more fundamental Dirac-Brueckner-Hartree-Fock theory. The energy per nucleon together with the symmetric isoscalar potentials for three different DBHF sets were fitted, together with proton and neutron scalar and vector potentials. Isoscalar σ, ω mesons with their self-interactions, and isovector ρ, δ mesons with ρ-ω cross interaction were used as the degrees of freedom and parameters of the fit. Generally, a good reproduction of both the energy and the potentials was reached and thus the parameter sets are representing an effective DBHF description of asymmetric nuclear matter at normal baryon densities applicable for the calculation of finite nuclei properties as well. The cross interaction between ρ and ω mesons turned out to improve reproduction of properties of asymmetric nuclear matter. Additionally, it increases symmetry energy rise in common nuclei density region, i.e., bellow saturation density, and decreases its grow above the saturation point. It has consequences for properties of finite nuclei, especially with large isospin asymmetry, and also for description of nuclear matter at higher densities, relevant in high energy nuclear collisions and several astrophysical processes and phenomena (e.g., neutron star properties and supernovae explosions). Isovector δ meson also improves quality of the mean-field model but without such a strong impact on density dependence of symmetry energy. These results imply that $\rho - \omega$ cross interaction is very useful and important tool for a better description of nuclear matter and finite nuclei with high isospin asymmetry.

Due to extreme isospin asymmetries reached in recent high energy ion collisions and also due to higher accuracy observations of astrophysical phenomena enabling us to constraint some properties of nuclear matter, it is inevitable to examine proper extrapolations to higher density regions. One of the possibilities is considering of hyperon and lepton presence through modelling hyperon matter

in β-equilibrium. Their influence on composition of equilibrated hyperon matter and electron chemical potential is studied. Supporting previous conclusions, the results indicate that VCI is an important degree of freedom with distinct impact on both composition of matter and electron chemical potential. Since they soften nuclear equation of state, especially in δ meson presence they reduce hyperonization of matter and strengthen population of neutrons, thus making the neutron star matter more neutron-rich. Notwithstanding, they simultaneously strongly support hyperons in their role of kaon condensation reduction factor, resulting in lower saturation value of the electron chemical potential and also in its steeper downtrend after the hyperon onset, thus shifting kaon condensation appearance to even higher densities, and thus making neutron star matter more neutron-rich also from this point of view.

8 Outlook

A natural application of obtained parametrizations sets is calculation of finite nuclei properties that would offer further information about quality of the results and about their connection to experimentally verifiable reality.

Apart from that, in order to enable description of neutron star matter and matter in high energy collisions, it was inevitable to extrapolate calculations to higher density region. That has been performed by an inclusion of hyperons which are very likely to abound in neutron star cores as well as take part in high energy dynamics.

One of the next natural steps is an application of the results to calculation of neutron star properties, and thus obtaining additional constraints on mean-field parameters. Calculation of neutron star properties requires to have at our disposal the nuclear matter pressure which is directly following from energy density as its derivative with reflection to baryon density:

$$p = \rho_B^2 \frac{\partial}{\partial \rho_B}\left(\frac{\varepsilon}{\rho_B}\right) . \tag{70}$$

Next it is necessary to use the general relativity equation. Under condition of non-rotating neutron star with isotropic mass distribution (spherical symmetry) its structure is given by Tolman–Oppenheimer–Volkov (TOV) equations [168]

$$\frac{\partial p(r)}{\partial r} = -\frac{G[\rho(r) + p(r)/c^2][m(r) + 4\pi r^3 p(r)/c^2]}{r^2[1 - -2Gm(r)/rc^2} , \tag{71}$$

$$m(r) = \int_0^r 4\pi r'^2 \rho(r') dr' , \tag{72}$$

where $p(r)$ is pressure and $m(r)$ is gravitational mass inside radius r and G is gravitational constant. Starting at some central density ρ_c these equations have to be numerically integrated till $r = R$ is reached where the pressure is zero, thus obtaining star radius R and gravitational mass of the star $M = m(R)$.

Another interesting quantity directly observable and thus employable into

nuclear matter description improvement is the gravitational red shift on the star surface [169]:

$$z = [1 - 2M_G G/Rc^2]^{-1/2} - 1 \ , \tag{73}$$

where M_G is gravitational mass of the star given by Eqs. (71) and (72).

As it was already mentioned in the Introduction, these astrophysical quantities would provide additional empirical constraints on nuclear equation of state and parameters of the models, realizing thus interesting connection between microscopic world of the field theories and macroscopic world of the general relativity controlled phenomena, or virtually, a connection of entire quaternion of the fundamental forces known. This interesting topic has remained under development.

Acknowledgement

I would like to acknowledge my supervisor for his help without which this work could not be completed.

References

[1] L. I. Schiff, Phys. Rev. **84**, 1, 10 (1951).

[2] M. H. Johnson and E. Teller, Phys. Rev. **98**, 783 (1955).

[3] H. P. Duerr, Phys. Rev. **103**, 469 (1956).

[4] J. D. Walecka, Ann. Phys. (N.Y.) **83**, 491 (1974).

[5] B. D. Serot and J. D. Walecka, Adv. Nucl. Phys. **16**, 1 (1986).

[6] K. Wehrberger, R. Wittman, and B. D. Serot, Phys. Rev. C **42**, 2680 (1990).

[7] W. Baade and F. Zwicky, Phys. Rev., **45**, 138 (1934).

[8] R. Giacconi, H. Gursky, F. R. Paolini, and B. B. Rossi, Phys. Rev. Lett. **9**, 439 (1962).

[9] A. Hewish, S. J. Bell, J. D. H. Pilkington, P. F. Scott, and R. A Collins, Nature **217**, 709 (1968).

[10] J. A. McNeil, J. R. Shepard, and S. J. Wallace, Phys. Rev. Lett. **50**, 1439 (1983); J. R. Shepard, J. A. McNeil, and S. J. Wallace, Phys. Rev. Lett. **50**, 1443 (1983).

[11] H. Leutwyler, Ann. Phys. (N.Y.) **235**, 165 (1994).

[12] C. Ordonez, L. Ray, and U. van Kolck, Phys. Rev. C **53**, 2086 (1996).

[13] P. Hohenberg and W. Kohn, Phys. Rev. **136**, B864 (1964).

[14] R. Brockmann and R. Machleidt, Phys. Rev. **C 42**, 1965 (1990).

[15] V. R. Pandharipande, I. Sick, and P. K. A. deWitt Huberts, Rev. Mod. Phys. **69**, 981 (1997).

[16] N. Kaiser, S. Fritsch, and W. Weise, Nucl. Phys. A **700**, 343 (2002).

[17] W. D. Myers and W. J. Swiatecki, Ann. Phys. (N.Y.) **84**, 186 (1974).

[18] B. A. Brown and B. H. Wildenthal, Annu. Rev. Nucl. Part. Sci. **38**, 29 (1988).

[19] H. J. Mang, Phys. Rep. **18**, 325 (1975); A. L. Goodman, Adv. Nucl. Phys. **11**, 263 (1979).

[20] M. Kleban, B. Nerlo-Pomorska, J.-F. Berger, J. Decharge, M. Girod, and S. Hilaire, Phys. Rev. C **65**, 024309 (2002).

[21] M. Brack and P. Quentin, Phys. Lett. B **56**, 421 (1975).

[22] M. Centelles, M. D. Estal, and X. Vinas, Nucl. Phys. A **635**, 193 (1998).

[23] J. W. Negele and D. Vautherin, Phys. Rev. C **5**, 1472 (1972); Phys. Rev. C **11**, 1031 (1975).

[24] R. Brockmann and H. Toki, Phys. Rev. Lett. **68**, 3408 (1992).

[25] D. Vautherin and M. Veneroni, Phys. Lett. B **29**, 203 (1969).

[26] J. Decharge and D. Gogny, Phys. Rev. C **21**, 1568 (1980).

[27] P.-G. Reinhard and H. Flocard, Nucl. Phys. A **584**, 467 (1995).

[28] J. M. Pearson and M. Farine, Phys. Rev. C **50**, 185 (1994).

[29] S. A. Fayans, S. V. Tolokonnikov, E. L. Trykov, and D. Zawischa, Nucl. Phys. A **676**, 49 (2000).

[30] B. D. Serot and J. D. Walecka, Int. J. Mod. Phys. **E 6**, 515 (1997).

[31] R. Fritz, H. Muther, and R. Machleidt Phys. Rev. Lett. **71**, 46 (1993).

[32] A. R. Bodmer, Nucl. Phys. **A 292**, 703 (1991).

[33] S. Kubis and M. Kutschera, Phys. Lett B **399**, 191 (1997).

[34] H. Mueller and B. D. Serot, Nucl. Phys. **A 606**, 508 (1996).

[35] M. Rufa, P.-G. Reinhard, J. A. Maruhn, W. Greiner, and M. R. Strayer, Phys. Rev. C **38**, 390 (1988).

[36] J. Zimanyi and S. A. Moszkowski, Phys. Rev C **42**, 1416 (1990).

[37] R. Brockmann, Phys. Rev. C **18**, 1510 (1978).

[38] D. Von-Eiff, J. M. Pearson, W. Stocker, and M. K. Weigel, Phys. Rev. Lett. B **324**, 279 (1994).

[39] C. J. Horowitz and B. D. Serot, Phys. Lett. B **108**, 377 (1982).

[40] C. Speicher, R. M. Dreizler, and E. Engel, Ann. Phys. (N.Y.) **213**, 312 (1991).

[41] T. Burvenich, D. Madland, J. A. Maruhn, and P.-G. Reinhard, Phys. Rev. C **65**, 044308 (2002).

[42] F. Tonduer, Nucl. Phys. A **315**, 353 (1979).

[43] M. Serra and P. Ring, Phys. Rev. C **65**, 064324 (2002).

[44] D. L. Hill and J. A. Wheeler, Phys. Rev. **89**, 1102 (1953).

[45] M. Anguiano, J. L. Edigo, and L. M. Robledo, Nucl. Phys. A **696**, 467 (2001).

[46] Y. Nogami, Phys. Rev. B **134**, B313 (1964).

[47] P. Ring, P. Schuck, *The Nuclear Many-Body Problem* (Springer, New York) (1980).

[48] A. Kamlah, Z. Phys. **216**, 52 (1968).

[49] S. Marcos, H. Flocard, and P.-H. Heenen, Phys. Lett. B **134**, 287 (1984).

[50] E. Runge and E. K. U. Gross, Phys. Rev. Lett. **52**, 997 (1984).

[51] J. W. Negele, Rev. Mod. Phys. **54**, 913 (1982).

[52] D. Bohm and D. Pines, Phys. Rev. **92**, 609 (1953).

[53] W. J. Bertozzi, J. Friar, J. Heisenberg, and J. W. Negele, Phys. Lett. B **41**, 408 (1972).

[54] B. Friedmann and V. R. Pandharipande, Nucl. Phys. A **361**, 502 (1981).

[55] M. Bender, P.-H. Heenen, and P.-G. Reinhard, Rev. Mod. Phys. **75**, 121 (2003).

[56] M. Beiner, H. Flocard, N. Van Giai, and P. Quentin, Nucl. Phys. A **238**, 29 (1975).

[57] J. Bartel, P. Quentin, M. Brack, C. Guet, and H.-B. Hakansson, Nucl. Phys. A **386**, 79 (1982).

[58] J. Dobaczewski, H. Flocard, and J. Treiner, Nucl. Phys. A **422**, 103 (1984).

[59] E. Chabanat, P. Bonche, P. Haensel, J. Meyer, and R. Schaeffer, Nucl. Phys. A **635**, 231; **643**, 441(E) (1998).

[60] M. Samyn, S. Goriely, P.-H. Heenen, J. M. Pearson, and F. Tondeur, Nucl. Phys. A **700**, 142 (2002).

[61] J. Decharge and D. Gogny, Phys. Rev. C **21**, 1568 (1980).

[62] G. A. Lalazissis, J. Konig, and P. Ring, Phys. Rev. C **55**, 540 (1997).

[63] M. Bender, K. Rutz, P.-G. Reinhard, J. A. Maruhn, and W. Greiner, Phys. Rev. C **60**, 034304 (1999).

[64] S. Gmuca, in *Proc. 2nd Int. Conf. Fission and Properties of Neutron-Rich Nuclei*, St. Andrews, Scotland, June 28 - July 3, 1999, eds. J. H. Hamilton, W. R. Phillips, H. K. Carter, World Sci., Singapore, 2000, p. 75.

[65] D. Von-Eiff, W. Stocker, and M. K. Weigel, Phys. Rev. C **50**, 1436 (1994).

[66] K. Rutz, M. Bender, P.-G. Reinhard, and J. A. Maruhn, Phys. Lett. B **468**, 1 (1999).

[67] D. H. Rischke, Nucl. Phys. A **583**, 663 (1995).

[68] J. I. Kapusta, A. P. Vischer, and R. Venugopalan, Phys. Rev. C **51**, 901 (1995).

[69] H. Krivine, J. Treiner, and O. Bohigas, Nucl. Phys. A **336**, 155 (1980).

[70] P.-G. Reinhard, Z. Phys. A **329**, 257 (1988).

[71] P.-G. Reinhard, M. Rufa, J. A. Maruhn, W. Greiner, and J. Friedrich, Z. Phys. A **323**, 13 (1986).

[72] J. Friedrich and P.-G. Reinhard, Phys. Rev. C **33**, 335 (1986).

[73] R. J. Furnstahl and B. D. Serot, Phys. Rev. C **41**, 262 (1990).

[74] C. B. Dover, H. Feshbach, and A. Gal, Phys. Rev. C **51**, 541 (1995).

[75] G. Q. Li and C. M. Ko, Phys. Lett. B **351**, 37 (1995).

[76] K. Saito and A. W. Thomas, Phys. Rev. C **51**, 2757 (1995).

[77] S. Gayo, Y.-J. Zhang, and R.-K. Su, Nucl. Phys. A **593**, 362 (1995).

[78] C. M. Ko and G. Q. Li, Nucl. Phys. A **583**, 591 (1995).

[79] P. J. Elis, R. Knorren, and M. Prakash, Phys. Lett. B **349**, 11 (1995).

[80] J. Schaffner, A. Gal, I. N. Mishustin, H. Stocker, and W. Greiner, Phys. Lett. B **334**, 268 (1994).

[81] M. Jaminou, R. Mendez Galain, G. Ripka, and P. Stassaart, Nucl. Phys. A **537**, 418 (1992).

[82] K. Saito and A. W. Thomas, Phys. Lett. B **327**, 9 (1994).

[83] R.J. Furnstahl and B.D. Serot, Comments Nucl.Part.Phys. **2**, A23-A45 (2000).

[84] www.bnl.gov/RHIC

[85] www.cebaf.gov

[86] www.nscl.msu.edu

[87] www.triumf.ca

[88] www.ornl.gov

[89] www.ganil.fr

[90] www.cern.ch

[91] www.gsi.de

[92] www.phy.anl.gov/ria/

[93] www.riken.jp

[94] G. E. Brown, K. Kubodera, and M. Rho, Phys. Lett. B **192**, 273 (1987).

[95] M. van der Klis, Ann. Rev. Astron. Astrophys. **38**, 717 (2000).

[96] L. Burderi *et al.*, Astrophys. J. **560**, L71 (2001).

[97] M. Y. Fujimoto, and R. E. Taam, Astrophys. J. **305**, 246 (1986).

[98] R. C. Duncan and C. Thompson, Astrophys. J. **392**, L9 (1992).

[99] C. Y. Cardal, M. Prakash, and J. M. Lattimer, Astrophys. J. **554**, 322 (2001).

[100] M. H. Thoma, J. Trumper, and V. Burwitz, arXiv:astro-ph/0305249 (2003).

[101] F. Matera and A. Delliafiore, Phys. Lett. B **296**, 1 (1992).

[102] H. Huber, F. Weber, and M. K. Weigel, Phys. Rev. C **50**, R1287 (1994).

[103] K. Sumiyoshi, H, Toki, and R. Brockmann, Phys. Lett. B **276**, 393 (1992).

[104] F. Weber, arxiv:astro-ph/0207053, 2002, In *Proceedings of the VIII International Workshop on Hadron Physics*, April 14-19 2002, Rio Grande do Sul, Brazil.

[105] D. Kaplan and A. Nelson, Phys. Lett. B **175**, 57 (1986).

[106] J. C. Collins and M. J. Perry, Phys. Rev. Lett **34**, 1353 (1975).

[107] I. N. Mishustin, M. Hanauske, A. Bhattacharyya, L. M. Satarov, H. Stoecker, and W. Greiner, Phys. Rev. Lett. B **552**, 1 (2003).

[108] V. A. Ambartsumyan and G. S. Saakyan, Soviet. Astron. **4**, 187 (1960).

[109] A. A. Tyaokin, Sov. J. Nucl. Phys. **22**, 89 (1976).

[110] N. K. Glendenning, Astrophys. J. **293**, 470 (1985).

[111] F. Weber and M. K. Weigel, Nucl. Phys. A **493**, 549 (1989); A **505**, 779 (1989).

[112] M. Rufa, J. Schaffner, J. Maruhn, H. Stoecker, W. Greiner, and P.-G. Reinhard, Phys. Rev. C **42**, 2469 (1990).

[113] S. K. Ghosh, S. C. Phatak, and P. K. Saha, Z. Phys. A **352**, 457 (1995).

[114] C. Greiner and J. Schaffner-Bielich, published in *Heavy Elements and Related New Phenomena*, eds. R. K. Gupta, W. Greiner, World Sci.; nucl-th/9801062.

[115] M. Danysz and J. Pniewski, Phil. Mag. **44**, 348 (1953).

[116] D. J. Millener, C. B. Dover, and A. Gal, Phys. Rev. C **38**, 2700 (1988).

[117] W. Bruckner *et al.*, Phys. Lett. B **62**, 481 (1976).

[118] S. Polikanov, Nucl. Phys. A **478**, 805c (1988).

[119] C. J. Batty, E. Friedman, and A. Gal, Phys. Lett. B **335**, 273 (1994).

[120] J. Schaffner, C. B. Dover, A. Gal, C. Greiner, and H. Stoecker, Phys. Rev. Lett. **71**, 1328 (1993); Ann. of Phys. (N.Y.) **235**, 35 (1994).

[121] I. N. Filikhin and A. Gal, Phys. rev. C **65**, 041001 (2002).

[122] C. Albertus, J. E. Amaro, and J. Nieves, Phys. Rev. Lett. **89**, 032501 (2002).

[123] R. E. Chrien and C. B. Dover, Ann. Rev. Nucl. Part. Sci. **39**, 113 (1989).

[124] H. Bando, T. Motoba, and J. Zofka, Int. J. Mod. Phys. A **5**, 4021 (1990).

[125] N. K. Glendenning, Phys. Rev. C **64**, 025801 (2001).

[126] S. Balberg, I. Lichtenstadt, and G. B. Cook, Astro. J. Suppl. Series **121**, 515 (1999).

[127] P. Khaustov *et al.*, Phys. Rev. C **61**, 054603 (2000).

[128] F. Weber and N. K. Glendenning, astro-ph/9609074, published in the Brazilian Journal of Teaching Physics (1996).

[129] J. Boguta and A. R. Bodmer, Nucl. Phys. **A 292**, 413 (1977).

[130] S. Gmuca, J. Phys. G **17**, 1115 (1991); Nucl. Phys. A **547**, 447 (1992).

[131] B. Liu, V. Greco, V. Baran, M. Colonna, and M. Di Toro, Phys. Rev. C **65**, 045201 (2002).

[132] A. L. Fetter and J. D. Walecka: *Theoretical Mechanics of Particle and Continua*, MacGraw-Hill, New York (1980).

[133] J. Mares, E. Friedman, A. Gal, and B. K. Jennings, Nucl. Phys. A **594**, 311 (1995).

[134] K. A. Brueckner *et al.*, Phys. Rev. **110**, 431 (1958).

[135] R. Brockmann and R. Machleidt, Phys. Lett. B **149**, 283 (1984).

[136] B. ter Haar and R. Malfliet, Phys. Rep. **149**, 207 (1987).

[137] F. de Jong and H. Lenske, Phys. Rev. C **57**, 3099 (1998).

[138] C. Fuchs and H. Lenske, Phys. Rev. **C 52**, 3043 (1995).

[139] H. Q. Song, Z. X. Wang., and T. T. S. Kuo, Phys. Rev. C **46**, 1788 (1992).

[140] Hua-lin Shi and Bao-qui Chen, Phys. Rev. C **52**, 144 (1994).

[141] Zhon-gyu Ma, Hua-lin Shi, and Bao-qui Chen, Phys. Rev C **50**, 3170 (1994).

[142] W. Zuo, I. Bombacci, and U. Lombardo, Phys. Rev. C **60**, 024605 (1999).

[143] B. A. Li, C. M. Ko, and W. Bauer, Inter. J. Mod. Phys. E **7**, 147 (1998).

[144] P. E. Haustein, At. Data Nucl. Data Tables **39**, 185 (1988).

[145] R. Brockmann, G. Q. Li, and R. Machleidt, Phys. Rev. C **45**, 2782 (1992).

[146] C. H. Lee, T. T. S. Kuo, G. Q. Li, and G. E. Brown, Phys. Rev. C **57**, 3488 (1998); Phys. Lett. B **412**, 235 (1997).

[147] H. Huber, F. Weber, and M. K. Weigel, Phys. Lett. B **317**, 485 (1993); Phys. Rev. C **51**, 1790 (1995).

[148] http://cernlib.web.cern.ch/cernlib/

[149] K. Oyamatsu *et al.*, Nucl. Phys. **A634**, 3 (1998).

[150] B.A. Li, Phys. Rev. Lett. **88**, 19270 (2002); Nucl. Phys. **A 708**, 365 (2002); Nucl. Phys. **A 722**, 209 (2003).

[151] J. Rizzo, M. Colonna, M.Di Toro, and V. Greco, arXiv:nucl-th/0309032 (2003).

[152] S. Gmuca, Proc. Int. Symposium on Exotic Nuclei, Baikal, World Sci., (2001).

[153] M. Colonna, M.Di Toro, G. Fabri, and S. Maccarone, Phys. Rev. C **57**, 1410 (1998).

[154] R.J. Furnstahl, arXiv:nucl-th/0307111 (2003).

[155] B.A. Nikolaus, T. Hoch, and D.G. Madland, Phys. Rev. C **46**, 1757 (1992).

[156] T. Gaitanos, M.Di Toro, S. Typel, V. Baran, C. Fuchs, V. Greco, and H.H. Wolter, arXiv:nucl-th/0309021 (2003).

[157] V. Greco, M. Colonna, M.Di Toro, G. Fabri, and F. Matera, Phys. Rev. C **64**, 045203 (2001).

[158] B. Liu, V. Greco, V. Baran, M. Colonna, and M.Di Toro, Phys. Rev. C **65**, 045201 (2002).

[159] H. Huber, F. Weber, M. K. Weigel, and Ch. Schaab, Int. J. of Mod. Phys. E **7**, 301 (1998).

[160] I. Vidana, A. Polls, and A. Ramos, Phys. Rev. C **62**, 035801 (2000).

[161] F. Hoffman, C. M. Keil, and H. Lenske, Phys. Rev. C **64**, 025804 (2002).

[162] J. Schaffner and I. Mishustin, Phys. Rev. C **53**, 1416 (1996).

[163] J. M. Lattimer, C. J. Pethick, M. Prakash, and P. Haensel, Phys. Rev. Lett. **66**, 2701 (1991).

[164] G. Mao, P. Papazoglou, P. Hofmann, S. Schramm, H. Stoecker, and W. Greiner, Phys. Rev. C **59**, 3381 (1999).

[165] T. Waas, M. Rho, and W. Weise, Nucl. Phys. A **617**, 449 (1997).

[166] G. Q. Li, C. H. Lee, and G. E. Brown, Nucl. Phys. A **625**, 372 (1997); Phys. Rev. Lett. **79**, 5214 (1997).

[167] R. Barth *et al.*, Phys. Rev. Lett. **78**, 4027 (1997).

[168] S. L. Shapiro and S. A. Teukolsky, *Black Holes, White Dwarfs, and Neutron Stars: The Physics of Compact Objects* (Wiley, New York, 1983).

[169] R. B. Wiringa, V. Fiks, and A. Fabrocini, Phys. Rev. C **38**, 1010 (1988).